RESEARCH ON THE PROPERTIES OF AMORPHOUS SEMICONDUCTORS AT HIGH TEMPERATURES

John P. deNeufville

Energy Conversion Devices, Incorporated

Prepared for:

Advanced Research Projects Agency

17 June 1973

FOURTH SEMI-ANNUAL TECHNICAL REPORT

Contract DAHC15-70-C-0187

RESEARCH ON THE PROPERTIES OF AMORPHOUS SEMICONDUCTORS AT HIGH TEMPERATURES

Prepared by: Energy Conversion Devices, Inc.
1675 W. Maple Road
Troy, Michigan 48084

For: Advanced Research Projects Agency
[Order No. 1570; Program Code 0D10]

Contract Period: 18 May 1970 to 17 May 1973

Total Contract Price: $976,786.00

J. P. deNeufville
Program Technical Manager
313-549-7300

Copy No. 17

Unclassified
Security Classification

DOCUMENT CONTROL DATA - R&D
(Security classification of title, body of abstract and indexing annotation must be entered when the overall report is classified)

1 ORIGINATING ACTIVITY (Corporate author) Energy Conversion Devices, Inc. 1675 W. Maple Road, Troy, Michigan 48084	2a REPORT SECURITY CLASSIFICATION Unclassified 2b GROUP N/A

3 REPORT TITLE
RESEARCH ON THE PROPERTIES OF AMORPHOUS SEMICONDUCTORS AT HIGH TEMPERATURES

4 DESCRIPTIVE NOTES (Type of report and inclusive dates)
Fourth Semi-Annual Technical Report - 19 Dec 1971 to 18 May 1972

5 AUTHOR(S) (Last name, first name, initial)
deNeufville, John P.

6 REPORT DATE 17 June 1973	7a TOTAL NO OF PAGES ~~99~~ 107	7b NO OF REFS 53
8a CONTRACT OR GRANT NO. DAHC15-70-C-0187 b PROJECT NO. 1001/36 c. d.	9a ORIGINATOR'S REPORT NUMBER(S) 516-4 9b OTHER REPORT NO(S) (Any other numbers that may be assigned this report) None	

10 AVAILABILITY/LIMITATION NOTICES
The distribution of this report is unlimited

11 SUPPLEMENTARY NOTES Details of illustrations in this document may be better studied on microfiche.	12 SPONSORING MILITARY ACTIVITY Advanced Research Projects Agency Arlington, Virginia 22209

13 ABSTRACT

1. Measurement of T_g versus composition in the Ge-Se-Te system have revealed that the T_g singularity, which occurs at the fully cross-linked di-chalcogenide composition ($GeSe_2$) in the Ge-Se binary system, does not extend along the $GeTe_2$ - $GeSe_2$ line of chalcogen saturation in the ternary system, but rather deviates progressively towards Ge as Te is substituted for Se. This tendency appears to reflect the competitive effects of bond strength, as measured by band gap, and connectedness, as measured by the 8-N rule, in determining T_g.

2. A region of liquid immiscibility was discovered in the $GeSe_2$-$GeTe_2$-Te subsystem of the Ge-Se-Te ternary system. Tie lines appear to radiate from a $GeSe_2$-rich liquid toward a range of Te-rich Te-Se liquids. This immiscibility leads to the formation of 2-phase glasses for certain compositions in this region, and the T_g's and T_x's of each phase can be separately measured by scanning calorimetry.

3. This immiscibility tendency is termed "primary immiscibility" since it can be simply predicted as a topological consequence of the thermodynamic requirement of forming the lowest energy set of covalent chemical bonds. Thus $Ge_{20}Se_{40}Te_{40}$ or $GeSe_2Te_2$ can be regarded as a mixture of $GeSe_2$ and Te_2, which are constructed of Ge-Se and Te-Te chemical bonds respectively. Only by physically separating these two phases can one eliminate Se-Te, Ge-Te, Se-Se, and Ge-Ge bonds whose presence results in a demonstrable decrease in overall bonding energy.

4. We have observed copious nucleation of tiny Te crystals upon heating sputtered

DD FORM 1 JAN 64 1473

Unclassified
Security Classification

14. KEY WORDS	LINK A		LINK B		LINK C	
	ROLE	WT	ROLE	WT	ROLE	WT
Amorphous Semiconductors Amorphous Materials Chalcogenide Materials High Temperature Device Materials						

amorphous films of $Ge_{20}Se_{40}Te_{40}$, and we tentatively associate this phenomenon with the separation of a Te-rich liquid which spontaneously nucleates and crystallizes without the requirement of the familiar surface nucleation sites which characterize the nucleation and crystallization of most other telluride glass samples. Indeed, unlike other telluride alloys, the volume fraction of Te crystals depends on time and temperature alone, and not at all on film thickness.

5. The electrical and optical measurements of amorphous alloy phases in the Ge-Se-Te ternary system supply abundant evidence for chemical ordering for well annealed sputtered films of composition $GeTe_2$ and $GeSe_2$. Each of these alloys can be modeled by the SiO_2 structure with tetrahedral Ge and 2-fold chalcogen, a structure which contains only one chemical bond type (i.e., Si-O, Ge-Se, Ge-Te, etc.).

6. The thermopower of unannealed and annealed sputtered amorphous Ge-Se-Te films has been surveyed extensively, resulting in the discovery of a wide variety of n-type amorphous chalcogenide alloys among the annealed Se-rich and Ge-rich ternary alloy sputtered film samples. Numerous examples of initially p-type sputtered alloys which become n-type upon annealing at or below T_g have been discovered, leading to a wide variety of new electronic device possibilities. In addition to exposing these potential technological developments, the thermopower measurements have served a highly useful scientific role in characterizing the majority charge carriers as a function of alloy composition, state of annealing and temperature.

TABLE OF CONTENTS

TABLE OF CONTENTS (CONT.)

LIST OF FIGURES

LIST OF FIGURES (CONT.)

LIST OF TABLES

I. INTRODUCTION AND SUMMARY OF MAJOR ACCOMPLISHMENTS

1.1 Introduction

The overall emphasis in this research program has been the correlation of amorphous chalcogenide alloy composition and atomic structure on the one hand, and with thermal stability, electronic structure, and electrical and optical properties on the other hand. The Fourth and Fifth Semiannual Technical Reports analyze, respectively, two separate aspects of this problem: 1, the role of chemical clustering and ordering tendencies in controlling thermal and electronic properties; and 2, the role of thin film depositional parameters, illumination, and annealing in controlling the structural state and thus the electronic properties (primarily the optical properties) of amorphous films. No overall synthesis of composition - property relations for this immense new class of electronic and optical materials can be imagined prior to the establishment of these two fundamental types of information. In the present report, the role of chemical clustering and ordering is assessed for a prototypical three-component chalcogenide system, Ge-Se-Te. This system was chosen because it spans a wide range of materials parameters: T_g varies from ~0°C (for pure Te) to ~425°C (for $GeSe_2$), while E_{O4}, the photon energy at which the optical absorption coefficient attains the value 10^4 cm^{-1}, varies from ~0.8 eV (for Te) to ~2.4 eV (for $GeSe_2$). D.C. conductivity, broadly speaking, correlates with optical gap, although the subtle differences between the conductivity "gap" (twice the electrical activation energy) and the optical gap form the basis for interpreting the electronic band structure as a function of alloy composition

and state of annealing as presented in the Final Technical Report. Thermopower, on the other hand, is an extremely sensitive function of composition and the degree of annealing, shifting from p-type to n-type with annealing for some of the Ge and Se-rich alloys.

In addition to having a wide range of property variations, most of these ternary alloys can be relatively well characterized structurally. Pure amorphous Ge, for example, is well described by the Polk Model[51], while the binary Te-Se amorphous phases consist of copolymer 2-connected rings and chains.[10] $GeTe_2$ and $GeSe_2$ are usually assumed to be structural analoges to SiO_2, although the hard evidence for these assumptions obtained under the present research program[47,48] and elsewhere[50] is very recent. The issue of the structure of amorphous GeTe and the GeTe-GeSe alloys was examined in detail in our Third Semiannual Technical Report. Several collaborative efforts between ECD and their laboratories are currently under way to resolve the issue of the 3-fold model vs. the 2-fold Te and 4-fold Ge model.

Thus the property trends toward higher T_g's and larger band gaps with the substitution of Se for Te take place (again, with the possible exception of the less understood GeTe-GeSe structures) along isomorphous series whose structure depends, for the most part, on the Ge:X ratio rather than on the Se:Te ratio. Since the number of valence electrons per atom, n_e, varies continuously from 6 for the chalcogens Se and Te to 4 for pure Ge, this system encompasses the entire range of average valence electron concentration which leads to covalently bonded polymeric alloys. Values of n_e higher than 6 lead

to molecular materials with low thermal stability and unstable amorphous structures while values of n_e lower than 4 lead generally to metallicly bonded materials with low glass forming tendencies. We have felt it necessary to survey the properties of more complex ternary amorphous chalcogenide systems in order to obtain an overview of all of the factors which determine thermal stability and electronic properties, and these studies will be reviewed in the Final Technical Report. The present report, however, represents the most thorough study, to our knowledge, of a ternary chalcogenide system, and thus will be used as the starting point in attempting to analyze the more complex ternary systems.

In concluding this introduction, it should be noted that the technique of rf sputtering to deposit amorphous thin films has been a cornerstone of the technical approach we have utilized in these studies. When conductivities and vapor pressures vary over 10 decades or more at a given temperature, most other techniques of thin film deposition are inadequate for preparing homogeneous films ranging between 300Å (for transmission electron microscopy) to 100μm (for calorimetry and IR reflectivity studies) in thickness. Flash evaporation, slow thermal evaporation, co-evaporation, dc sputtering and other techniques have been successfully applied to some ranges of these sample requirements by ourselves (for cross-checking purposes) and by others. Many of these latter techniques do present certain advantages compared to rf sputtering, most noticeably in the area of oxygen, nitrogen and argon contamination, which can, of course, be essentially eliminated by evaporation

under UHV conditions. However it has been our goal to prepare amorphous films of as wide a variety of compositions as possible and to characterize these films in terms of properties like optical gap and glass transition temperature, which are largely insensitive to trace impurities.

A further word on the rf sputter deposition of multi-component chalcogenide alloys is required to characterize compositional fidelity of the sputtered films with respect to the nominal hot-pressed cathode compositions. We have used electron microprobe to analyze films sputtered along the Ge-Te binary join and along the $GeSe_2$-$GeTe_2$ pseudo-binary join. The accuracy of these experiments was somewhat limited by the difficulty of obtaining homogeneous bulk materials for use as reference standards. However, taking these difficulties into consideration we can simply summarize the results of these studies by stating that the measured concentrations of the elemental components were within 1 - 2% of the stated compositions, depending on concentration. For example a thin film of GeSeTe or $Ge_{33.3}Se_{33.3}Te_{33.3}$ would be expected to have the composition $Ge_{33.3\pm1}\ Se_{33.3\pm1}\ Te_{33.3\pm1}$. The actual analysis for one sample of that film was $Ge_{34\pm1}Se_{32\pm1}Te_{34\pm1}$, where the ±1% now represents the accuracy of the analysis itself. This is a typical result, indicating the difficulty of ascertaining highly accurate knowledge of chemical composition using this method of analysis. We thus relied on the nominal composition as the measure of film composition throughout these studies, recognizing that this assumption introduces a small uncertainty into the results thereby obtained. Furthermore, our analysis of the role of dc bias

in determining both argon entrappment and stoichiometric deviations for sputtered $GeTe_2$, which will be presented in the Final Technical Report, provides an additional warning regarding small compositional fluctuations from sputtered sample to sample which may arise from differnces of induced dc bias depending on minute details of sputtering procedure and substrate type. These differnces tend to be troublesome only for materials like $GeSe_2$ whose properties depend so sensitively on stoichiometry and whose high resistivity accentuates the possibility of self-biasing effects.

1.2 Summary of Major Accomplishments

1. Measurements of T_g versus composition in the Ge-Se-Te system have revealed that the T_g singularity, which occurs at the fully cross-linked di-chalcogenide composition ($GeSe_2$) in the Ge-Se binary system, does not extend along the $GeTe_2$ - $GeSe_2$ line of chalcogen saturation in the ternary system, but rather deviates progressively towards Ge as Te is substituted for Se. This tendency appears to reflect the competitive effects of bond strength, as measured by band gap, and connectedness, as measured by the 8-N rule, in determining T_g. In the Ge-Te system, the Ge-Ge bonds are stronger than the Ge-Te bonds, while in the Ge-Se system the reverse is true. Thus the highest T_g in the Ge-Te system presumably occurs at Ge (although this cannot be experimentally verified bacause T_x occurs below T_g between $GeTe_2$ and Ge) whereas the highest value of T_g in the Ge-Se system occurs at $GeSe_2$.

2. A region of liquid immiscibility was discovered in the $GeSe_2$-$GeTe_2$-Te subsystem of the Ge-Se-Te ternary system. Tie lines appear to radiate from a $GeSe_2$-rich liquid toward a range of Te-rich Te-Se liquids. This immiscibility leads to the formation of 2-phase glasses for certain compositions in this region, and the T_g's and T_x's of each phase can be separately measured by scanning calorimetry.

3. This immicibility tendency is termed "primary immiscibility" since it can be simply predicted as a topological consequence of the thermodymic requirement of forming the lowest energy set of covalent chemical bonds. Thus

$Ge_{20}Se_{40}Te_{40}$ or $GeSe_2Te_2$ can be regarded as a mixture of $GeSe_2$ and Te_2, which are constructed of Ge-Se and Te-Te chemical bonds respectively. Only by physically separating these two phases can one eliminate Se-Te, Ge-Te, Se-Se, and Ge-Ge bonds whose presence results in a demonstrable decrease in overall bonding energy. Of course entropic effects are significant, so that, for example, the $GeSe_2$-rich phase of $Ge_{20}Se_{40}Te_{40}$ contains roughly 13 atomic percent Te.

4. The chemical bonding origins of this immiscibility indicate that the phase separating glasses containing the most Te-rich low T_g phase should lie along the join connecting Te and $GeSe_2$, e.g., $Ge_{20}Se_{40}Te_{40}$. Pure liquid Te cannot be supercooled by any known method to form a glass, presumably because of homogeneous nucleation of crystals during the quench. Thus the separation of a very Te-rich liquid at temperatures well below the Te melting point leads to the possibility for homogeneous nucleation of Te crystals in that liquid. We have observed copious nucleation of tiny Te crystals upon heating sputtered amorphous films of $Ge_{20}Se_{40}Te_{40}$, and we tentatively associate this phenomenon with the separation of a Te-rich liquid which spontaneously nucleates and crystallizes without the requirement of the familiar surface nucleation sites which characterize the nucleation and crystallization of most other telluride glass samples. Indeed, unlike other telluride alloys, the volume fraction of Te crystals depends on time and temperature alone, and not at all on film thickness. We feel that this observation may be unique among amorphous chalcogenide

films, and may have practical consequences for situations requiring the presence of electrically conducting particles in an essentially non-conducting matrix.

5. The electrical and optical measurements of amorphous alloy phases in the Ge-Se-Te ternary system supply abundant evidence for chemical ordering for well annealed sputtered films of composition $GeTe_2$ and $GeSe_2$. Each of these alloys can be modeled by the SiO_2 structure with tetrahedral Ge and 2-fold chalcogen, a structure which contains only one chemical bond type (i.e., Si-O, Ge-Se, Ge-Te, etc.). Along the join Ge-SeTe the optical and electrical gaps both peak sharply for annealed films at the di-chalcogenide GeSeTe composition, indicating a high degree of chemical order for that alloy as well. Here, however, both Ge-Se and Ge-Te bonds are concluded to be present, and, thus the alloys are disordered with respect to the distribution of these two bond types but are ordered with respect to the exclusion of the other 4 possible bond types (Ge-Ge, Se-Se, Te-Te and Se-Te). These results confirm our earlier speculation concerning local order in the amorphous $GeSe_2$-$GeTe_2$ alloy system, and support our earlier conclusion that these pseudo-binary alloys do not phase separate.[3]

6. The thermopower of unannealed and annealed sputtered amorphous Ge-Se-Te films has been surveyed extensively, resulting in the discovery of a wide variety of n-type amorphous chalcogenide alloys among the annealed Se-rich and Ge-rich ternary alloy sputtered film samples. Numerous examples of initially p-type sputtered alloys which become n-type upon

annealing at or below T_g have been discovered, leading to a wide variety of new electronic device possibilities. In addition to exposing these potential technological developments, the thermopower measurements have served a highly useful scientific role in characterizing the majority charge carriers as a function of alloy composition, state of annealing, and temperature.

2. GLASS FORMATION AND PHASE SEPARATION IN THE GeSe-GeTe-Se-Te SYSTEM

2.1 Introduction

The chalcogen and chalcogenide glasses are well known to exhibit covalent bonding, and the valency satisfaction model of Mott[1] is the standard point of departure in interpreting electrical or optical properties of these glasses. This model, and the nearly equivalent random covalent model,[2] assumes that each constituent atom in the glass forms 8-N covalent bonds where N is the number of valence electrons. The identification of these bonds in the Mott model is left vague, while the random covalent model assumes that a random statististical distribution of all possible covalent bond types will occur. By contrast, various ordered covalent models have also been proposed[3] which consider the effect of relative bond strengths in calculating the distribution of bond types, and can lead to complete chemical ordering at certain stoichiometric ratios such as $GeSe_2$, SeTe, etc.

X-ray structural studies of chalcogenide glasses using the Radial Distribution Function (RDF) technique confirm the covalent nature of the chemical bonds, both with regard to bond length[4] and with regard to average coordination number as predicted by the 8-N rule for each atom. Thus the valency satisfaction model, which was created to account for the absence of impurity band conduction in amorphous chalcogenide alloys, is thoroughly confirmed by the X-ray studies which have been performed.

Unfortunately the X-ray studies do not successfully address the question of chemical ordering, and the observed RDF functions can be fitted by a variety of models including chemically ordered covalent models, random covalent models,

and even completely phase separated models, so long as each elemental component retains its 8-N coordination. An additional problem arises by the inability of RDF analysis to distinguish whether the 8-N coordination applies for individual atoms or whether an average 8-$\bar{N}$ coordination applies where $\bar{N}$ is the average valence number per atom. For example RDF analysis cannot yet distinguish between a 4 fold Ge - 2 fold Te structure for amorphous GeTe versus a 3 fold Ge - 3 fold Te structure.[5] Hopefully more sophisticated diffraction experiments will resolve these questions, but in the meantime other measurements will play some role for determining nearest neighbor bonding within the constraints of covalent bonding models.

The Ge-Te-Se system can be decomposed into two sub-systems: Ge-$GeSe_2$ - $GeTe_2$ and $GeSe_2$ - $GeTe_2$ - Se - Te along the line of so-called "chalcogen saturation",[3] $GeSe_2$ to $GeTe_2$. While this study is primarily concerned with the behavior of glasses in the latter, "excess chalcogen" subsystem, some measurements from the former "chalcogen deficient" sub-system are presented as well. The chalcogens Se and Te have S^2P^4 valence electron configuration and thus form 2 covalent bonds each. Ge is S^2P^2, or SP^3, when hybridized, thus forming 4 covalent bonds tretrahedrally distributed in space.[6] Both Se[7] and Te[8] form isomorphous hexagonal crystals with Se_n and Te_n polymeric chains along their C axes, and these chain structures are preserved in the glasses,[9] although Se glass contains a substantial proportion of Se_8 rings as well.[10] As Ge is added to Se or Te glass, these chains become cross linked in the sense that each Ge atom uses its four bonds to connect two chalcogen chains. If Ge retains its four-fold coordination, and

Se and Te retain their two-fold coordination, and no Ge-Ge bonds are formed, then this cross linking process becomes fully saturated at the GeX_2 compositions which then contain only Ge-X bonds. These compositions are thus called chalcogen saturated, in that no chalcogen-chalcogen bonds exist for the completely ordered case.

The concept of average coordination number or average connectedness is useful in understanding this cross linking process and the effects which accompany the addition of further germanium beyond that necessary for chalcogen saturation, i.e. in understanding the chalcogen deficient portion of the Ge-Te-Se system. In this study, $C = 8 - \bar{N}$, where $\bar{N}$ is the average number of valence electrons per atom, will be interchangeably termed average connectedness or average coordination number. C provides a measure of the degree to which the glass forms a three dimensional network and provides some index of the strength of that network. For example, for $N = 7$, $C = 1$, we have an unconnected network or a molecular solid, such as Cl_2, etc. For $N = 6$, we have $C = 2$ which leads to chains as in the cases of Se and Te. Of course for $C = 2$ we can have unconnected structures like Se_8 rings, but these are a perturbation of the simple theory and will be disregarded for simplicity at this stage of description.

Examples of glasses with $\bar{N} = 5$ and $C = 3$ are amorphous As and Sb, and binary materials like GeTe and GeSe. The question for the binary materials is whether the value of C is the average of half of the atoms having $C = 4$ (Ge) and half having $C = 2$ (Se, Te) or whether each atom has $C = 3$. Some

thermal measurements from our laboratories[12] in the Ge-Te system indicate a strong possibility for the 3-3 rather than the 4-2 network for amorphous GeTe but the question remains unresolved.

The group of glasses with $\bar{N} = 4$, $C = 4$ include amorphous Ge,[13] Si,[14] SiC[15] and appear to have the highest glass transition temperatures for a given value of bond strength.[16] Higher values of C appear to be unattainable, since 4 covalent bonds per atom lead to the highest possible number of bonding valence electrons per atom(8).

There appears to be a trade-off between bond strength and connectedness in determining the value of T_g for a given material. Rockstad and de Neufville[16] have shown that at constant bond strength, T_g increases with C, while at constant N, T_g increases with bond strength. These competing effects would be expected to be operative in complex systems like Ge-Te-Se and indeed are to be expected in binary systems like Ge-Se where C changes all the way from 2(Se) to 4(Ge) and the bond strength also varies strongly with composition.

The theoretical relationship between network connectedness, bond strength and T_g has only been analyzed in a few simple cases,[11] and no general analysis of the problem is known to the author. For $C = 2$ materials such as Se, analogies can be made to the behavior of organic polymers where T_g can be derived in some simple cases by knowledge of the chain length and the presence or absence of side groups.[17] The plasticizing by Se_8 rings bears sufficient analogies to effects in organic systems that some rigorous analysis is possible.[18] For these materials, viscous flow does

not require breaking any covalent bonds; the chains shear past each other by segmental motions during viscous flow. Since T_g is defined as the temperature at which the viscosity $\eta = 10^{13}$ Poise (in c.g.s. units), clearly T_g can be viewed in terms of a viscosity effect.

Semi-quantitative models for viscous flow exist for the tetrahedral random network liquids like GeO_2 and SiO_2.[19] Here the liquid has no weak bonds, so that some rearrangements among the strong covalent bonds are required for viscous flow. The viscosity in such cases appears to be thermally activated with a single activation energy which closely approximates the bond energy.

The intermediate cases between chain-like polymers (Se_n and Te_n) and fully cross-linked tetrahedral networks ($GeSe_2$ and $GeTe_2$) clearly represent some sort of an average of these two limiting cases. That is, as the cross-linking component Ge is added to Se or Te the viscosity will predictably rise and T_g will increase.

The only crystalline compound in the Ge-Te system is GeTe, which has a distorted NaCl structure and is thus not bonded covalently in contrast to GeTe glass.[4] GeSe has a comparable crystal structure,[20] involving an

orthorhombic distortion of the NaCl structure. $GeSe_2$ has a distorted version of the CdI_2 structure,[20] and is thus more ionically than covalently bonded.

Ordering tendencies are significant in the Ge-Se and Ge-Te systems while they are less predominant in the Se-Te system. The heat of formation of GeSe crystals is 9.85 k cal/gm atom[20] vs. 4.0 k cal/gm atom[20] for GeTe. These ordering tendencies persist in the Ge-Te glasses[12] but have not been quantitatively determined for the Ge-Se glasses. In Section 2.5.1 of this Report the energies of the possible covalent bond types will be calculated using the Pauling electronegativity criterion in lieu of more quantitative experimental information.

Ordering and clustering tendencies are always intimately related in structural chemistry, because each type of departure from a totally random structure implies the possibility of departures in the other direction: chemically ordered configurations tend to cluster relative to other chemically ordered configurations leading to regions of clustering separating regions of chemical order.[24] Thus phase separation is to be expected in any multicomponent amorphous system, and many references to phase separation in chalcogenide systems have appeared in the literature.[25,26,27,28] By phase separation liquid-liquid immiscibility is implied, where the

immiscibility should rigorously be a sub-liquidus metastable phenomenon. However the rigorous definition is not particularly useful since liquidus temperatures are not well known in multi-component systems, so phase separation and liquid immiscibility will be used here interchangeably.

In spite of all these qualitative observations of phase separation and even 2-T_g behavior[28] in one system, no thorough study of one single chalcogenide system has ever been reported which attempts to define the immiscibility tie lines and interpret the immiscibility tendency in chemical bonding terms.

2.2 Limits of Glass Formation

This study concerns the properties of amorphous semiconducting alloy phases in a portion of the Ge-Te-Se ternary system. The primary emphasis has been placed upon the compositional dependence of the glass transition temperature. In order to obtain fully amorphous samples, a variety of experimental techniques were utilized. The results of these efforts are listed in Table 2.1, which identifies the alloy compositions investigated, indicates what method or methods were successfully utilized to produce fully amorphous samples if any, and tabulates the glass transition temperature or temperatures obtained by DSC. In addition, these investigated compositions are mapped in the Ge-Se-Te ternary system in Figure 2.1.

Note that five categories of alloys are represented in Table 2.1. These categories are as follows:

1. No amorphous phase obtained by any method
2. Homogeneous glass obtained
   a. Single value of T_g indicating no phase separation
   b. $T_x < T_g$, so T_g cannot be measured
   c. Two values of T_g, Tg_1 and Tg_2, indicating phase separation
   d. $Tx_1 < Tg_1$ but $Tx_2 > Tg_2$; Tg_1 cannot be measured but Tg_2 can be measured.

In general no glass formation (category 1) means only that the amorphous phase was not obtained by the methods employed. In

TABLE 2.1

COMPOSITION, METHOD OF GLASS PREPARATION AND GLASS TRANSITION TEMPERATURE FOR Ge-Te-Se ALLOYS

Composition (%)			Method of Preparing Glass			T_g	T_x
Ge	Te	Se	Water Quench	Spray Cooling	rf Sputtering	(^oC)	(^oC)
70	30	-			x	-	352
60	40	-			x	-	268
50	50	-			x	-	232
45	55	-	x			Cry.	
40	60	-			x	-	208
36.7	63.3	-			x	-	220
33.3	66.7	-			x	230	
66.7	33.3	-	x			Cry.	
30	70	-			x	213	
25	75	-			x	190	
22	78	-		x		162	
20	80	-			x	159	
17	83	-			x	145	
				x		148	
15	85	-	x			Cry.	

TABLE 2.1 CONT.

Composition (%)			Method of Preparing Glass			T_g	T_x
Ge	Te	Se	Water Quench	Spray Cooling	rf Sputtering	(^oC)	(^oC)
10	90	-			x	105	
7.5	92.5	-	x			Cry.	
5	95	-			x	100	
2	98	-	x			Cry.	
-	100	-			x	Cry.	
				x		Cry.	
-	90	10		x		Cry.	
-	80	20		x		Cry.	
-	70	30		x		Cry.	
-	60	40		x		Cry.	
-	50	50			x	57	
-	40	60		x		75	
-	25	75			x	65	
-	16	84			x	59	
	12	88			x	56	
	10	90			x	55	
	8	92		x		54	
	4	96			x	47	

TABLE 2.1 CONT.

Composition (%)			Method of Preparing Glass			T_g	T_x
Ge	Te	Se	Water Quench	Spray Cooling	rf Sputtering	(^oC)	(^oC)
-	-	100	As			45	
10	-	90	x			95	
20	-	80	x			168	
30	-	70	x			364	
33.3	-	66.7	x			422	
					x	408	
35	-	65	x			423	
40	-	60	x			302	
50	-	50			x	324	
50	25	25			x	272	
40	30	30		x		296	
38	31	31		x		302	
36	32	32		x		295	
33.3	33.3	33.3		x		292	
					x	288	
32	34	34		x		282	
30	35	35		x		270	
27	36.5	36.5		x		260	

TABLE 2.1 CONT.

Composition (%)			Method of Preparing Glass			T_g	T_x
Ge	Te	Se	Water Quench	Spray Cooling	rf Sputtering	(^oC)	(^oC)
25	37.5	37.5		x		236	
22	39	39		x		208	230
						354	360
20	40	40			x	-	142
						340	350
18	41	41		x		-	-
						320	334
16	42	42	x			-	165
						284	340
15	42.5	42.5		x		105	157
						292	330
10	45	45		x		110	180
						280	-
5	47.5	47.5		x		86	
33.3	60	6.7		x		242	
33.3	53.3	13.3		x		217	
33.3	50	16.7		x		254	
33.3	46.7	20			x	260	

TABLE 2.1 CONT.

Composition (%)			Method of Preparing Glass			T_g	T_x
Ge	Te	Se	Water Quench	Spray Cooling	rf Sputtering	(^oC)	(^oC)
33.3	40	26.7			x	282	
25	65	10	x			201	
25	55	20	x			210	
45	25	30	x			208	
20	75	5	x			168	
20	60	20	x			169	
15	80	5	x			138	
15	75	10	x			140	
10	80	10	x			Cry.	
30	5	65	x			375	
25	10	65	x			252	
20	15	65	x			190	
20	10	70	x			175	
15	20	65	x			145	
15	10	75	x			135	
10	25	65	x			105	
10	10	80	x			102	
5	30	65	x			82	
5	10	85	x			78	

Fig. 2.1

Mapping of preparation method and investigated alloys in the Ge-Te-Se system where: circles represent materials quenched from the liquid state, triangles represent spray cooled materials and squares represent sputtered materials.

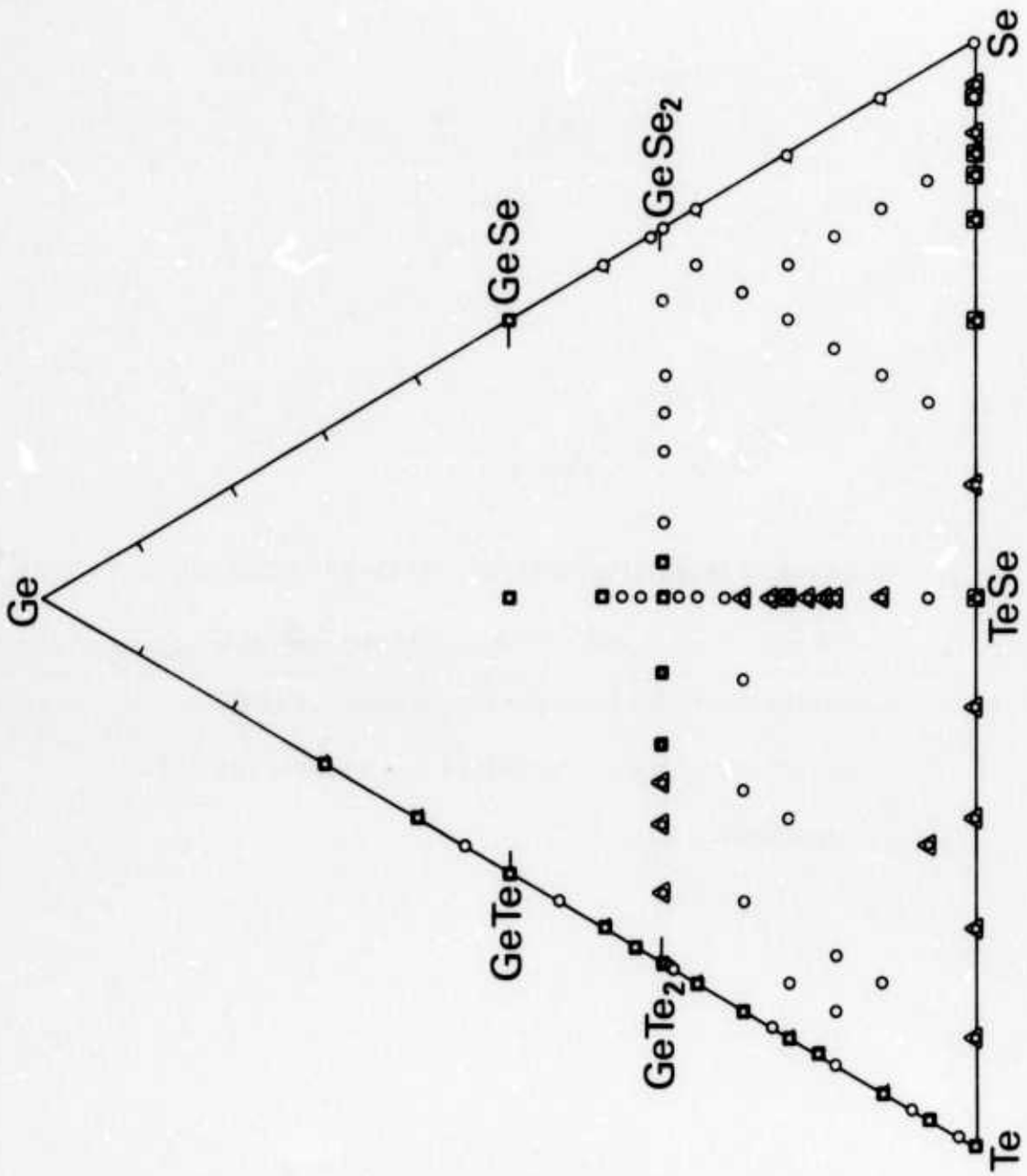
Ge
GeSe
GeSe2
Se
GeTe
GeTe2
TeSe
Te

some cases, i.e. pure Te and Te rich alloys, neither spraying nor r.f. sputtering at 25°C sufficed to give an amorphous sample, although both evaporation[9] and r.f. sputtering[30] on LN_2 cooled substrates can produce the amorphous phase. A distinction is often drawn between amorphous alloys produced by quenching, spray-cooling or splat cooling of the liquid phase (called glasses) as contrasted to alloys which cannot be prepared as glasses by continuous cooling of the liquid phase and must be evaporated or sputtered, etc. to form the amorphous solid phase (called non-crystalline solids). In this system that distinction appears to be arbitrary, in the sense that T_g's obtained on amorphous sputtered films (outside the phase-separating regime) are in good agreement with T_g's obtained on sprayed or quenched glasses where the two values can be directly compared.

The distinction between category 2a and category 2b appears to reflect significantly different behavior. In the case of amorphous films which crystallize before reaching T_g, T_g is not experimentally observable. Additionally, the physical properties of such films depend on the annealing history and no fully annealed state is available, since annealing at T_g is the normal prescription for eliminating the defects incorporated in amorphous films during deposition.[31]

Glasses produced in category 2c result in fine scale phase separated materials exhibiting a two T_g phenomena. That is, each phase has a distinctive glass transition temperature and crystallization temperature. These materials lie entirely within the Ge-Te-Se ternary system and are

thermodynamically bounded by a single phase homogeneous glass typical of category 2a.

A special case of category 2c is observed in category 2d where one amorphous phase nucleates and crystallizes spontaneously as soon as compositional fluctuations exceed some limit. As temperature is increased, concentration fluctuations develop within the homogeneous amorphous phase, which eventually coalesce into separate phases. At this point the metastable Te-rich phase finds itself in the vicinity of T^*, its homogeneous nucleation temperature, and rapidly crystallizes (see Section 3.4).

2.3 Compositional Dependence of T_g

2.3.1 Binary Systems

Glass transition temperature data for amorphous materials observed in the Ge-Te system are plotted in Figure 2.2. The Te rich portion of the diagram exhibits typical single phase homogeneity with steadily increasing glass transition temperatures as a function of increasing Ge content until the stoichiometric composition $GeTe_2$ is reached. For a two component system the amorphous phase at T_g must be homogeneous if T_g changes with composition.[25,3] At $GeTe_2$, T_x becomes less than T_g which limits DSC observation of the T_g at higher Ge concentrations. This observation conflicts with our earlier measurement[3] of T_g for the alloy $Ge_{38}Te_{62}$, which result is now considered to be in error.

Fig. 2.3 combines existing glass transition data of Nemilov[32] and Feltz, Büttner et. al.[33] with current data for glass transition temperatures as a function of composition for high Se compositions in the Ge-Se binary system. It is noted that the data obtained by Feltz, Büttner et. al. were

Fig. 2.2

Metastable portion of Ge-Te phase diagram where Tg is represented by circles and Te represented by squares.

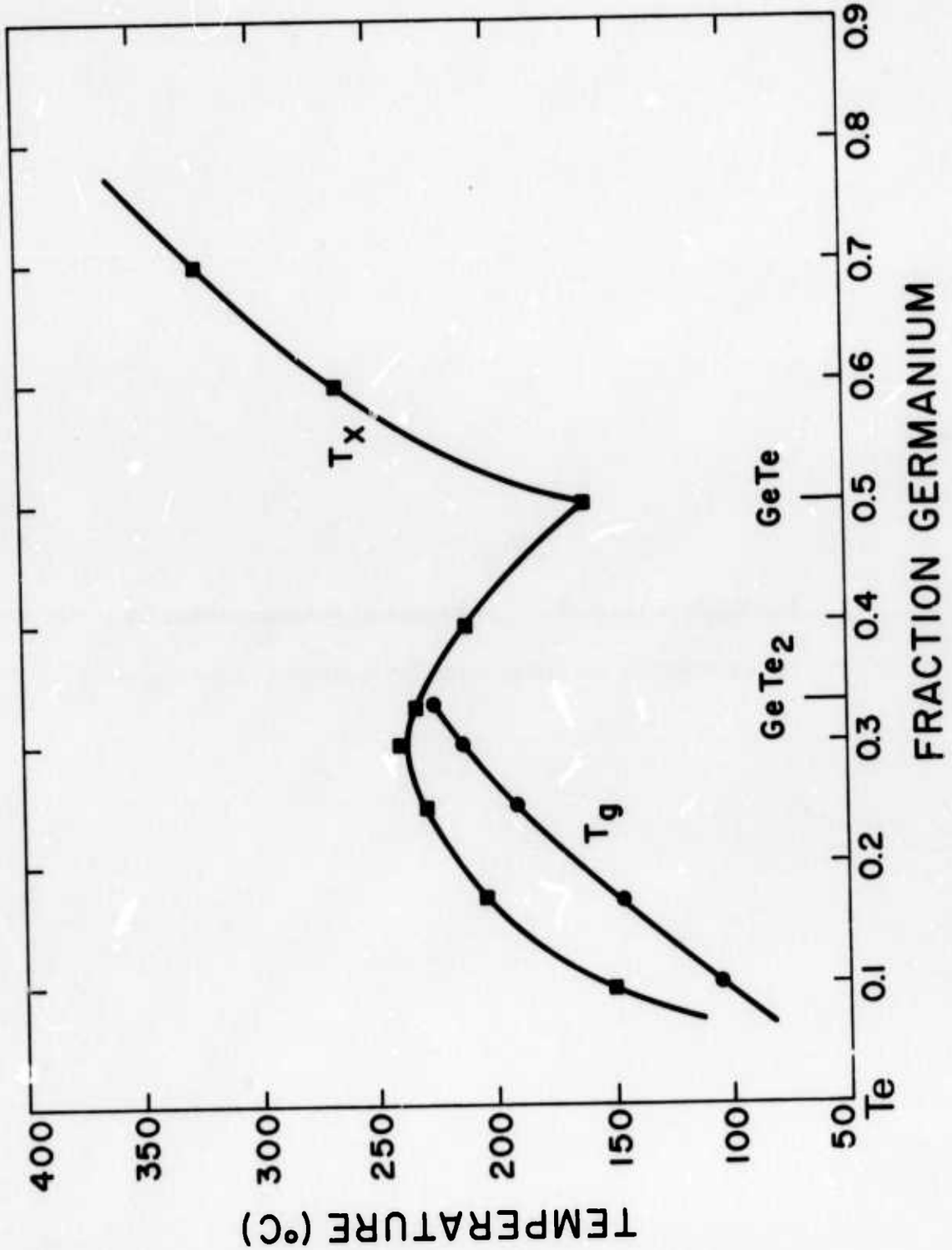
TEMPERATURE (°C)
400
350
300
250
200
150
100
50
Te
0.1
0.2
0.3
0.4
0.5
0.6
0.7
0.8
0.9
GeTe2
GeTe
FRACTION GERMANIUM
Tx
Tg

Fig. 2.3

Glass transition temperature in the Ge-Se binary system: solid circles from this study; open circles from reference 28; squares from reference 39.

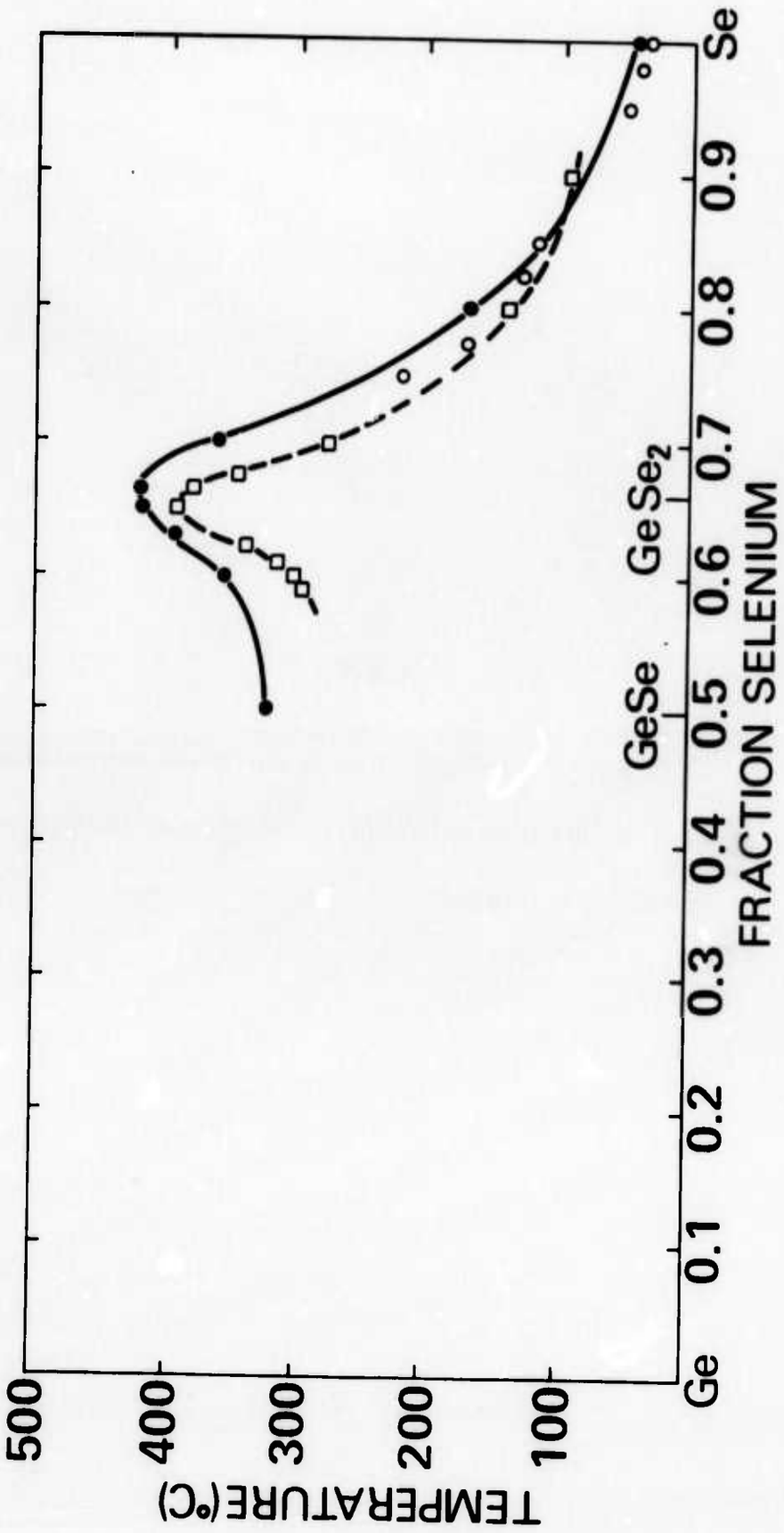
TEMPERATURE(°C)
500
400
300
200
100
Ge
0.1
0.2
0.3
0.4
0.5
0.6
0.7
0.8
0.9
Se
GeSe
GeSe2
FRACTION SELENIUM

taken by differential thermal analysis measurements at 4°C/min. scanning rates or less. The glass transition temperature peaks at or near the toichiometric composition $GeSe_2$. Similar results have been reported by Kawamoto and coworkers[34] for the Ge-S system and by Myers and Felty[35] at As_2S_3 in the As-S system. These binary T_g singularities occur at chalcogen saturated compositions where complete chemical ordering (i.e., Ge-Se bonds only) can occur, and where the chalcogen rings and chains can become fully cross linked by the cross linking additive (i.e. Ge in this case). When additional Ge is added to the chalcogen saturated or fully cross linked $GeSe_2$ composition, a decrease in T_g is observed.

Existing data has been extended in this system by means of r.f. sputtering to include the $Ge_{50}Se_{50}$ composition. T_g values for pure $GeSe_2$ were measured on samples obtained both by liquid quenching and by r.f. sputtering. These T_g data, which are listed in Table 3.1, are in relatively good agreement, and the lower T_g value for the sputtered film may be attributable to a slight deviation of stoichiometry associated with the sputtering process.

It is interesting to note that as Ge is added to pure Se, T_g increases more rapidly than when Ge is added to pure Te, as can be seen by a comparison of Figures 3.2 and 3.3. This portion of both systems has been viewed in terms of the cross linking of the chalcogen chains, and this cross linking thus appears to be more effective in the Ge-Se system than in the Ge-Te system.

The compositional dependency of T_g for the Se-Te system is plotted in Figure 2.4. The glass transition temperature increases gradually in the Se rich portion of the Se-Te system with increasing Te content toward a shallow maximum at approximately $TeSe_2$. From $TeSe_2$ to TeSe, T_g gradually decreases. The glass forming region is reduced in the Te rich portion of this system as compared to that of Ge-Te system. As amorphous TeSe and crystalline Te were the only sputtered compositions in this system, it is not known how much additional Te could be added to TeSe and still yield a glass which is stable at 25°C.

2.3.2. Pseudo-Binary Systems

The compositional dependence of the glass transition temperature in the pseudo-binary $GeTe_2$-$GeSe_2$ system is plotted in Figure 2.5 These results have been previously published.[3] This is a chemically and structurally simple system in the sense that both end members presumably share the fully cross linked random network structure observed for SiO_2[36], GeO_2[37] and similar glasses. Again, the typically smooth monotonic increase of T_g with the addition of $GeSe_2$ is suggestive of single phase homogeneity. The non-linearity of T_g with composition in the vicinity of pure $GeSe_2$ indicates that the addition of a small amount of $GeTe_2$ substantially decreases the glass transition temperature. This is analogous to the lowering of the SiO_2 glass transition temperature with addition of small amounts of GeO_2.[38]

Fig. 2.4

Glass transition temperature in the Se-Te binary system.

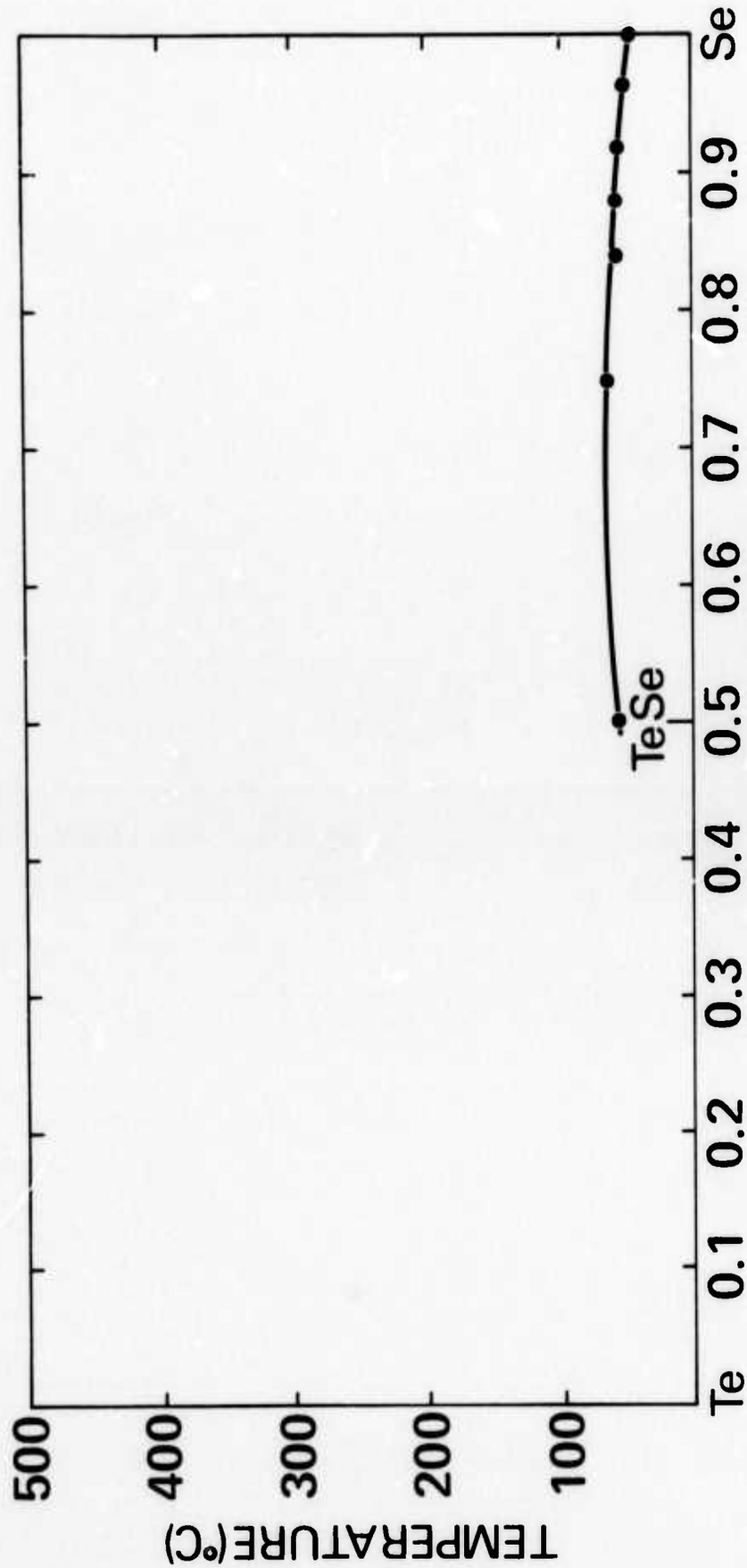
TEMPERATURE(°C)
500
400
300
200
100
Te
0.1
0.2
0.3
0.4
0.5
0.6
0.7
0.8
0.9
Se
FRACTION SELENIUM
TeSe

Fig. 2.5

Glass transition temperature in the $GeTe_2$-$GeSe_2$ psudo-binary system from reference 3.

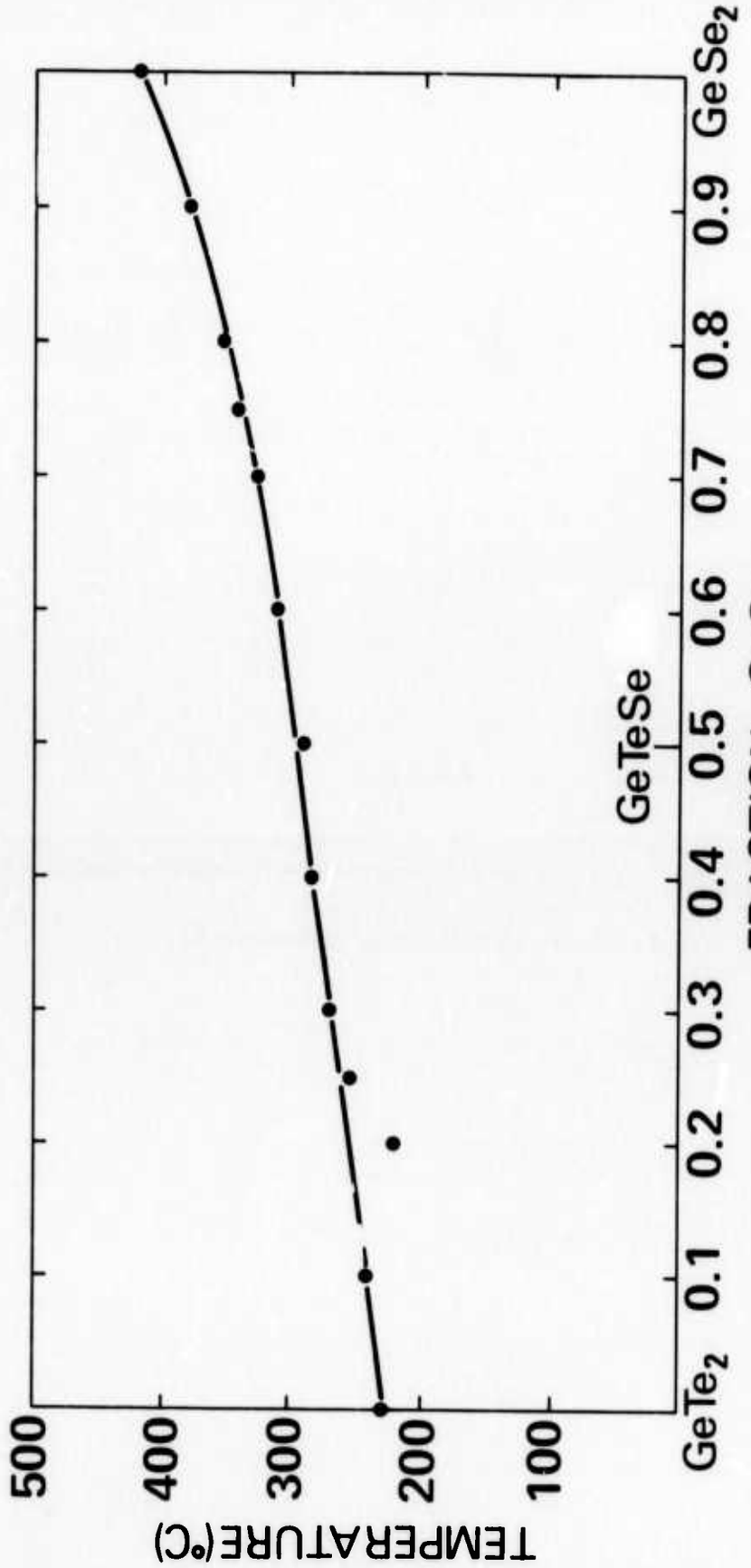
TEMPERATURE(°C)
500
400
300
200
100
GeTe2
0.1
0.2
0.3
0.4
GeTeSe
0.5
0.6
0.7
0.8
0.9
GeSe2
FRACTION GeSe2

The glass transition temperature decreases continuously from GeSe toward GeTe in the pseudo-binary system GeSe-GeTe. These data are plotted in Figure 2.6. Again at GeTe, T_x is less than T_g, making T_g unobtainable with calorimetric techniques, so that T_g values between GeTe and Ge_2SeTe are extrapolated.

The compositional dependence of T_g along the chalcogen rich portion of the pseudo binary system Ge-SeTe is an example of a glass forming system exhibiting two glass transition temperatures. These data are plotted in Figure 2.7. Within the miscibility gap, two distinct glass transitions are noted; one of substantially lower temperature than the other. The two-phase region is completely surrounded by a single phase homogeneous glass. The two-phase region between TeSe and GeTeSe returns to a single homogeneous phase at both end members. Both phases show a sharp increase in T_g from SeTe with addition of Ge. In the steeply varying regime between TeSe and GeTeSe, the addition of Ge to either phase increases the degree of cross-linking with a resulting rise in glass transition temperature.

2.3.3. Ternary System

Within the single phase region T_g isotherms are drawn to indicate regions of constant temperature glass transitions. This can be seen in Figure 2.8 where these isotherms show a continuous decline in T_g radiating from the T_g maximum of 422°C at the stoichiometric composition $GeSe_2$. This decline is very steep at first, becomes more gradual and then becomes

Fig. 2.6

Glass transition temperature, represented by circles, and crystallization temperature, represented by boxes, in the GeTe-GeSe psudo binary system.

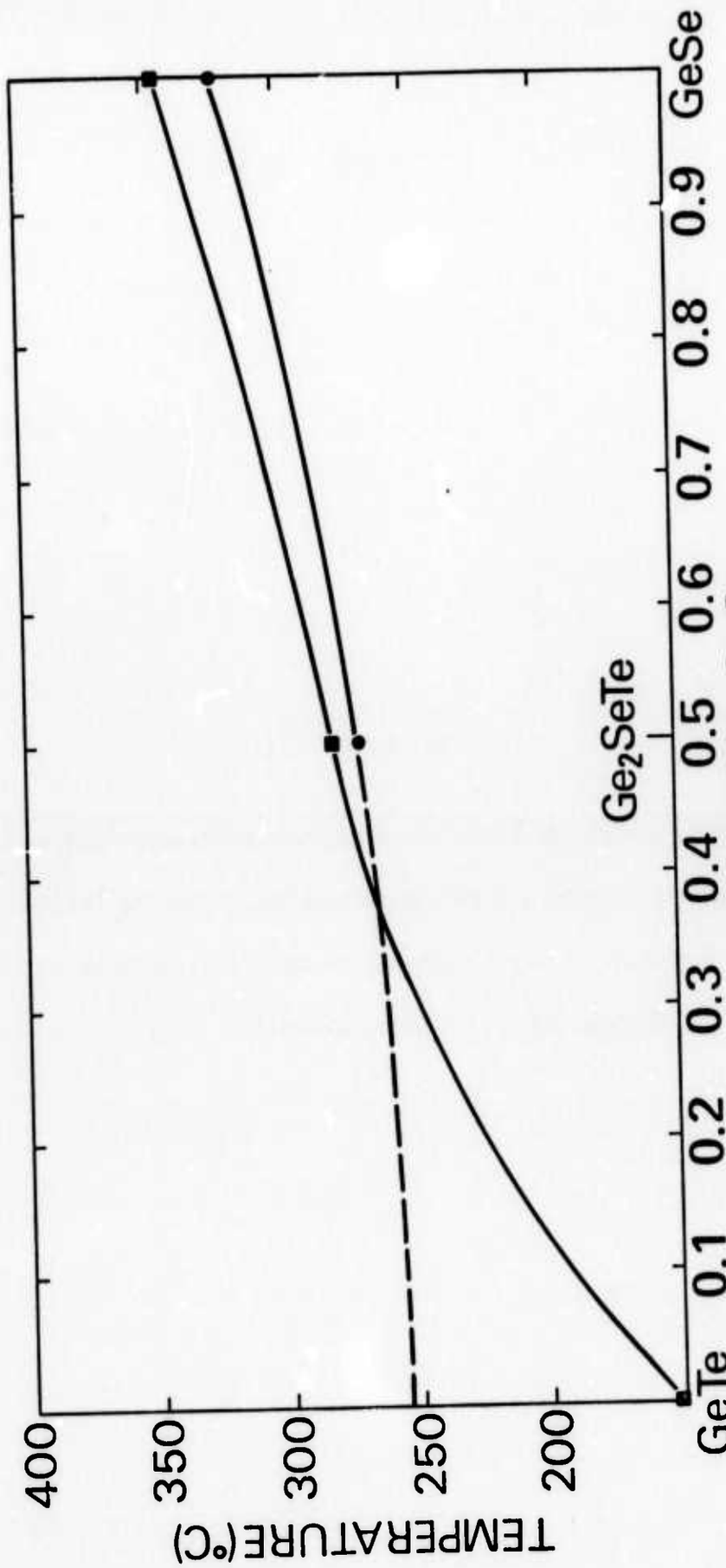
TEMPERATURE(°C)
400
350
300
250
200
GeTe
0.1
0.2
0.3
0.4
0.5
0.6
0.7
0.8
0.9
GeSe
Ge2SeTe
FRACTION GeSe

Fig. 2.7

Glass transition temperature and crystallization temperature showing the two-phase region of the Ge_2TeSe-TeSe psudo-binary system where Tg is represented by solid circles and Tx by open circles.

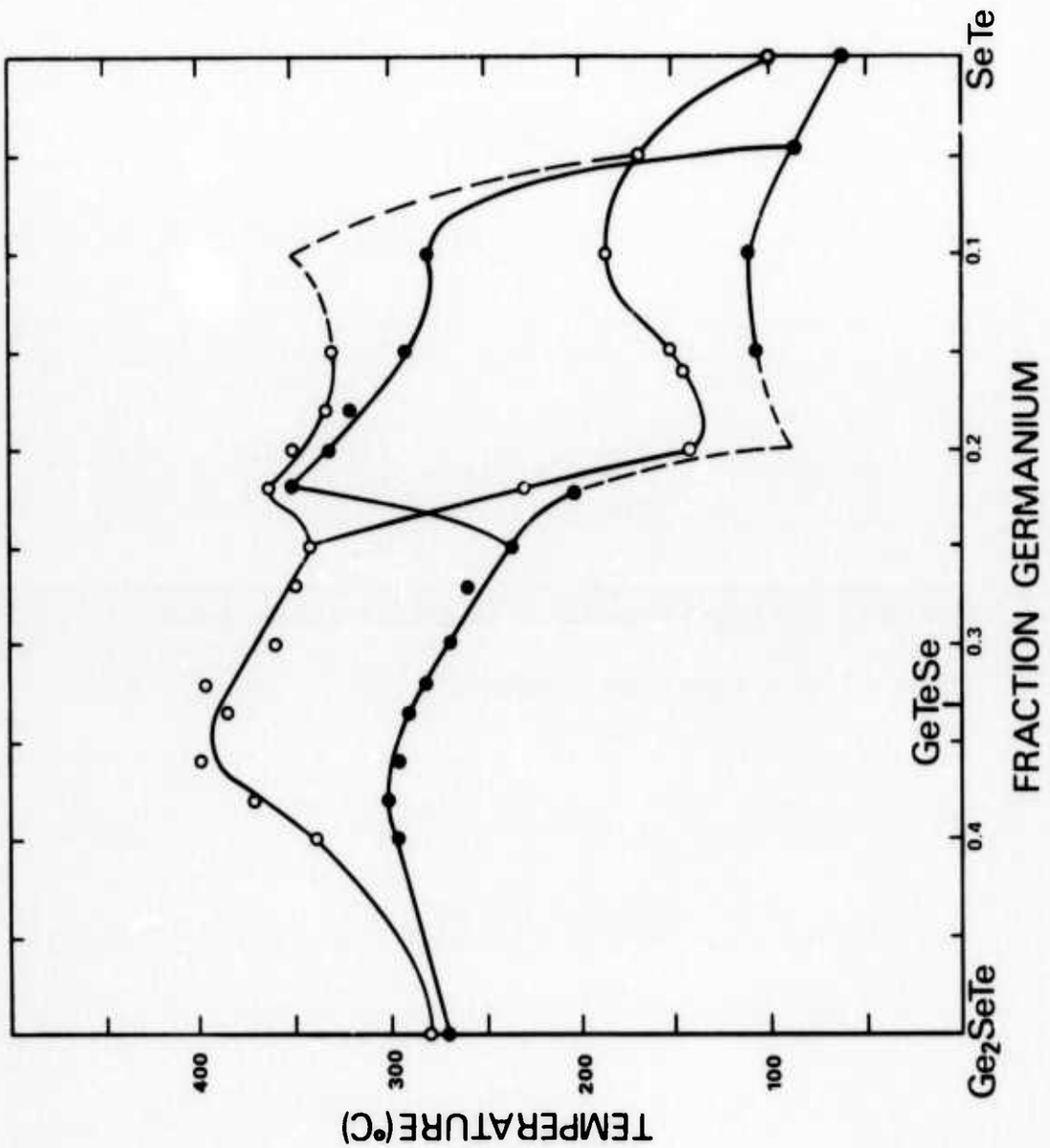
TEMPERATURE (°C)
400
300
200
100
Ge2SeTe
GeTeSe
Se Te
0.4
0.3
0.2
0.1
FRACTION GERMANIUM

Fig. 2.8

Glass transition temperature isotherms and tie lines in the Ge-Te-Se ternary system.

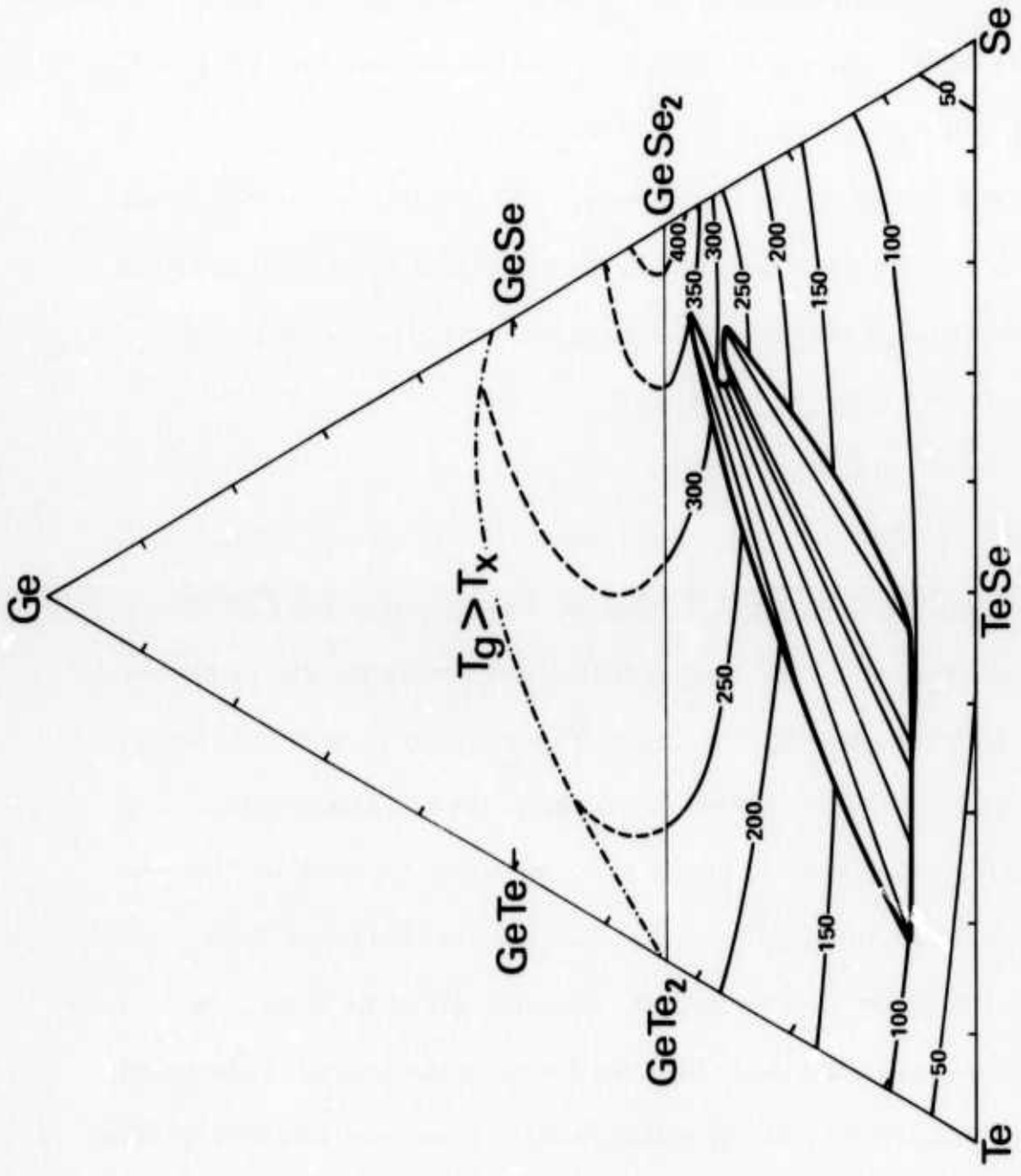
Ge
GeSe
GeSe2
Se
GeTe
GeTe2
Te
TeSe
Tg>Tx
400
350
300
250
200
150
100
50

nearly flat within the chalcogen-rich regions of the system. The T_g maxima for an increasing Te/Se ratio start at $GeSe_2$, and curve away from the chalcogen saturated $GeSe_2$-$GeTe_2$ pseudobinary, perhaps curving towards GeTe, although the line of T_g maxima crosses into the $T_x < T_g$ regime at a composition of roughly $Ge_{45}Te_{45}Se_{10}$.

The curvature of the isotherms near the Ge-Se join between Se and Ge_{25}-Se_{75} are consistent with the lower slope of T_g vs. Ge content in this portion of the Ge-Se system as compared to the Ge-Te system.

2.4 Evidence for Phase Separation

2.4.1 Construction of Tie Lines

No T_g isotherms are plotted in the two phase region, although, in a sense, the tie lines are T_g isotherms, lines along which both values of T_g are invariant. The compositions of the coexisting glassy phases in this portion of the ternary system are plotted so as to best fit the pair of T_g values at the boundaries of the two phase and homogeneous glass forming regions at the end points of the tie lines. In practice this procedure was simplified by using tie lines which radiate from $GeSe_2$, which appeared to fit the data as well as any other set of tie lines. The compositions used to define these tie lines lie along the join Ge-TeSe within the two-phase region; higher accuracy might have been obtained by using a modified version of the method of Mazurin[46] and plotting tie lines between compositions which share the same values of Tg_1 and Tg_2 within the two-phase region.

In the two-phase region, tie lines are used to connect the compositions of the two "coexisting" glassy phases obtained by the particular quenching method employed. These are thus not truly isothermal liquid-liquid "tie-lines" in the thermodynamic sense, since the liquid-liquid equilibrium is frozen during quenching at some particular composition values (corresponding to some unknown temperature). If all samples could be equilibrated at some $T >$ any Tg_2, say at $400^{\circ}C$, for a long time (without crystallization which is probably not possible) and then quenched to $25^{\circ}C$ with no further compositional changes, then the coexisting compositions thus obtained from the two T_g data points would give the coexisting isothermal ($400^{\circ}C$) liquid-liquid phase equilibrium.

2.5 Discussion and Conclusions

2.5.1 Analysis of T_g vs X Behavior in the GeSe-GeTe-Se-Te System

Primary emphasis has been placed on relating the compositional dependence of glass transition temperatures, phase separation behavior, and thermal crystallization to achieve some basic insight into the role of chemical ordering and network connectedness[8] in the glass forming region of the Ge-Te-Se system.

From calculations of bond strengths and random network connectedness for various stoichiometric compositions within the ternary system, it is possible to estimate relative T_g's. The glass transition temperatures, phase separating tendencies and crystallization behavior of amorphous Ge-Te-Se alloys can best be understood by reference to the bond energies of the six possible covalent types: Ge-Ge, Se-Se, Te-Te, Ge-Se, Ge-Te and Se-Te. Energies of individual bond strengths utilizing the Pauling electronegativity criterion are calculated below.

Table of Bond Energies[6]

A. homopolar single bonds

bond type	bond energy (K cal/E_A bond)
Ge-Ge	37.6
Se-Se	44.0
Te-Te	33.0

B. heteropolar single bonds

1. Pauling[6] Electronegativity Scale

element	electronegativity (X)
Ge	1.8
Se	2.4
Te	2.1

Assuming the arithmetic mean approximates the geometric mean, Pauling[6] calculates the bond energy (E_{AB}) as

$$E_{AB} = 1/2\ (E_{AA} \text{ and } E_{BB}) + 23\ (X_A - X_B)^2$$

Calculating the heteropolar single bonds gives:

bond type	bond energy E_{AB} (K cal/bond)
Ge-Se	49.08
Ge-Te	37.37
Se-Te	40.57

Rearranging the six bond types by descending energies results in the following order:

bond type	bond energy (K cal/bond)
Ge-Se	49.08
Se-Se	44
Se-Te	40.57
Ge-Ge	37.6

bond type	bond energy (K cal/bond)
Ge-Te	37.37
Te-Te	33

In the Ge-Te and Ge-Se chalcogen systems, T_g singularities occur at or near stoichiometric compositions. These singularities are strongly suggestive of an SiO_2 type tetrahedral random network of covalent bonds involving a high degree of chemical ordering. These binary system T_g singularities occur at chalcogen saturated compositions where the chalcogen rings and chains have become cross-linked by Ge. Additional amounts of Ge beyond this saturation limit result in either a sharp decrease in T_g, as in the case of the Ge-Se system at $GeSe_2$ or termination of the T_g effect (i.e. $T_x < T_g$), as in the case of the GeTe system at $GeTe_2$ The critical concentration of Ge which is sufficient to completely cross-link the chalcogen polymer chains appears at GeX_2, assuming no bonds between like atoms.

It is noted in Figure 2.2 that in the Ge-Te system the maximum T_g does not occur at the same stoichiometry as the only binary crystalline phase. This singularity in T_g does not correspond to the stable crystalline phase as in the case of $GeSe_2$, indicating that the glassy solid state does not always correspond to the structural chemical properties of the crystalline state.

Viscosity at T_g is, by definition, $\eta = 10^{13}$ poise.

In an SiO_2 type liquid, the covalent bonds must be broken to permit viscous flow. But viscosity, in the region of high viscosity, is most affected by weak links of low chemical bond energy. Based on the calculation of chemical bond energies, in the case of the fully cross-linked $GeTe_2$-$GeSe_2$ pseudo-binary system, Ge-Te bonds (37.37 K cal) are considered weaker than Ge-Se bonds (49.08 K cal). This gives rise to the non-linearity in T_g as $GeSe_2$ is approached from $GeTe_2$ seen in Figure 3.5.

In addition to cross-linking of the chalcogen atoms by the Ge atoms, the role of structural dissimilarities within a single component can lead to a significant contribution toward compositional dependencies of the glass transition temperature. This is seen in the Te-Se system where Se_8 molecules tend to lower viscosity as compared to Se_n chains. A. Eisenberg[18] calculates T_g to be equal to ~100°C for a pure chain Se liquid composed of equal chain lengths, while the actual T_g of amorphous Se containing a mixture of chains and rings is 45°C. Since pure Te has no ring components, Se_8 or possible Se_6Te_2[10] are the only stable rings in the binary Se-Te glasses. The shallow peak observed at or near $TeSe_2$ in the Te-Se binary system as shown in Figure 3.4, may possibly be explained in terms of ring-chain effects by assuming that the T_g matrix corresponds to the composition at which the ring (plastisizer) concentration increases rapidly with increasing Se.

In the Ge-Te system T_g increases with Ge content in the observable range of T_g as shown in Figure 3.2. The addition of Ge to Te increases both the bond strength and the connectedness,

continuously from pure Te to pure Ge. Thus C varies from 2 at pure Te to 4 at pure Ge, while Te-Te bonds (33 K cal) are replaced by Ge-Te bonds (37.4 K cal) between Te and $GeTe_2$.

A progressive reduction of the monomer Se_8 ring component by the addition of Ge atoms would tend to increase T_g. However, the observed rise in glass transition temperature in the Ge-Se system in Figure 3.3 is well past the limit which could be attributable merely to the elimination of rings. This observed increase in T_g is consistent with the model of progressive cross linking of chalcogen polymer chains with Ge in 4-fold coordination introducing a chain cross-linking point. A direct analogy can be made between the Ge-Se system and the Ge-Te system in terms of cross-linking effects. In Ge-Te, T_g rises linearly with atomic percent Ge between $Te_{90}Ge_{10}$ and $Te_{66.6}Ge_{33.3}$ ($GeTe_2$), while in the same portion of the Ge-Se system T_g increases very non-linearly. In fact at 10 percent Ge, the T_g in the Ge-Te system is ~105°C while the T_g in the Ge-Se system is ~84°C. These compositions have the same connectedness and the Se system has uniformly stronger bonds, so this result is surprising. Nor can the elimination of Se_8 rings with progressive Ge additions be invoked as a source of the discrepancy since the elimination of rings should cause T_g to increase more rapidly with increasing Ge. Perhaps clustering of the Ge atoms into fully cross-linked highly viscous regions separated by fluid Se-rich regions is the operative mechanism here. Glass transition isotherms in the homogeneous portion of the ternary Ge-Te-Se system in Figure 2.3 reflect the same cross-linking effects of Ge which

occur in the binary systems. Glass transition temperatures are increasing non-linearly from the chalcogen members toward the fully cross-linked $GeTe_2$ - $GeSe_2$ pseudo-binary join as the network connectedness increases. Along this pseudo-binary join $GeTe_2$-$GeSe_2$ of constant connectedness, T_g increases toward the higher bond strength $GeSe_2$. For intermediate compositions (i.e. compositions within the single phase regions but not falling along binary or pseudo-binary joins) effects of bond strength and network connectedness both contribute to determining the value of T_g. The observable T_g maximum occurs at 422°C at $GeSe_2$ where C = 2.66 and the bond strength (Ge-Se) is 49.08 K cal/bonds. Thus bond strength effects dominate C effects at this composition. With the addition of further Ge atoms to $GeSe_2$, weaker Ge-Ge bonds are added as C is increased. At first the bond strength effect dominates the C effect, and T_g decreases. Perhaps between GeSe and Ge this process is reversed and T_g again rises, but the present results do not address this possibility.

In addition to the increase in C from 2.66 at $GeTe_2$ to 4 at Ge, the effect of adding Ge atoms to $GeTe_2$ is compounded by the increase in bond strength ($E_{Ge-Ge} > E_{Ge-Te}$). Both these effects predict an increase in T_g beyond $GeTe_2$ toward Ge but since $T_x < T_g$ in this regime, this prediction cannot be experimentally verified. In the ternary system, the T_g maximum occurs at $GeSe_2$ while the ternary T_g maxima are decreasing and moving away from the line of chalcogen saturation as the Se/Te ratio decreases. This line defines the balancing condition between the bond energy effect and the connectedness effect. Interpretation of directionality of these balancing

condition maxima is difficult in the chalcogen deficient portion of the system due to insufficient data, but preliminary results indicate a maxima radiating out from $GeSe_2$ and terminating at Ge. The complexity of connecting this line of T_g maxima has some analogy to the T_g behavior observed in the Si-Te-As system[11] where the T_g maxima occur on a ridge connecting Si-Te to As.

2.5.2 Analysis of Ordering and Separating Tendencies

The region of liquid immiscibility or phase separation within the chalcogen-rich region of the Ge-Te-Se system exhibits for the most part a two T_g glass forming regime. With the possible exception of the homogeneous nucleation results of $Ge_{20}Te_{40}Se_{40}$ the two phase region is well behaved in terms of two phase glass formation. Most compositions studied within this region consisted of a low temperature amorphous phase which exhibited a Tg_1 and Tx_1 distinct from the high temperature phase.

A rough calculation can be made to determine the energy of $Ge_{20}Te_{40}Se_{40}$ in the randomly bonded and phase separated state. These assumptions will give an appropriate estimate for the thermodynamic tendency to form $GeSe_2$ plus Te clusters versus a completely randomly bonded glass at low temperatures (i.e. considering enthalpy only and ignoring entropy effects).

There are four orbitals per Ge

two orbitals per Se

two orbitals per Te

Number of orbitals in $Ge_{20}Te_{40}Se_{40}$

(0.20)(4) = 0.8 Ge orbitals

(0.40)(2) = 0.8 Se orbitals

(0.40)(2) = 0.8 Te orbitals

Total orbitals/atom = 2.4

Total number of bonds/atom = $\frac{\text{orbitals}}{\text{atoms}} \times \frac{\text{bonds}}{\text{orbitals}}$ =

2.4 x 1/2 = 1.2

of these 1.2 bonds there are

$\left(\frac{.8}{2.4}\right)\left(\frac{.8}{2.4}\right)\ 1.2$ Ge-Ge bonds etc.

Bond energy for a random model of $Ge_{20}Te_{40}Se_{40}$

Ge-Ge = (1/9)(1.2)(37.6 K cal/bond) = 5.01 K cal/bond

Ge-Te = (2/9)(1.2)(37.37 Kcal/bond) = 9.97 K cal/bond

Ge-Se = (2/9)(1.2)(49.08 K cal/bond) = 13.09 K cal/bond

Se-Se = (1/9)(1.2)(44.0 K cal/bond) = 5.87 K cal/bond

Se-Te = (2/9)(1.2)(40.57 K cal/bond) = 10.82 K cal/bond

Te-Te = (1/9)(1.2)(33.0 K cal/bond) = 4.40 K cal/bond

Total bond energy per g atom = 49.15 K cal

Bond energy for a clustered model of $Ge_{20}Te_{40}Se_{40}$ consisting of ordered $GeSe_2$ and Te clusters

Ge-Se = 39.26 K cal/bond

Te-Te = 13.20 K cal/bond

Total energy per g atom = 52.46 K cal

From rough calculations using Pauling's criteria for electronegativity it is shown that an ordered structure is thermodynamically more stable than a random structure by (52.46 - 49.15) K cal/g atom or 3.31 K cal/g atom. This relatively large energy difference predicts the phase separated structure for $Ge_{20}Te_{40}Se_{40}$, assuming no large differences in entropy of the two structures which is reasonable at these moderate temperatures. The resulting theoretical calculations of thermodynamic stability based on individual bond energies are experimentally verified in Figure 3.8 which shows $Ge_{20}Te_{40}Se_{40}$ in the heart of the phase separated region.

In using a modified version of Mazurin's[36] method for determining isothermal tie lines within a metastable phase separating region certain limitations and restrictions should be noted. Mazurin takes the Tg_1 isotherms within a region of phase separation as the directions of the tie lines. This method is thus limited to determining only the tie line and not its end points. Measuring both values of T_g within the phase separating region can give the tie line directions and their end points by comparison of the two T_g values with the T_g values outside the region of phase separation. The locus of the end points of these tie lines defines the boundary between the homogeneous and the phase separating regions. It is noted that even the composition $Ge_{20}Te_{40}Se_{40}$ does not reach either pure $GeSe_2$ or pure Te, indicating that some energy-entropy compromise for phase equilibrium is reached. It is noted that Tg_2 varies little with Ge:SeTe ratio of average composition but Tg_1 is very sensitive to average composition, consistent with tie lines radiating from near $GeSe_2$. Unfortunately, Tg_1

cannot be measured for this interesting composition, which may lead to further evidence of Te being the low viscosity phase.

When r.f. sputtered and spray cooled samples of $Ge_{20}Te_{40}Se_{40}$ are compared, they give very similar Tg_2 results, indicating that nearly the same equilibrium is attained whether separation occurs during heating or cooling.[39] Mazurin states that the composition of the low glass transition temperature phase for two-phase glasses stays in equilibrium with the surface of the high Tg phase, but that otherwise the equilibrium can be frozen because diffusional processes may be quite slow in the high viscosity phase. If large viscosity differences exist after phase separation has occurred, it may take considerable time for the phases to equilibriate during cooling. This may lead to erroneous conclusions utilizing a relative volume approach for the determination of tie lines. Possible limitations of taking T_g measurements to determine tie lines may arise from the unknown role of thermal history. Since equilibrium is not reached for all temperatures during quenching from the liquid, compositional fluctuations based on diffusional barriers may be set up. If this is indeed the case, only the high T_g phase could show compositional fluctuations due to viscosity and diffusional effects on quenching whereas the low temperature phase would remain fixed or frozen in composition. This phenomenon may account for the non-uniform appearance of the high temperature boundary between homogeneous and phase separated regions near $GeSe_2$ in Figure 2.8.

3. CRYSTALLIZATION OF SPUTTERED $Ge_{20}Se_{40}Te_{40}$

3.1 Introduction

Examination of material along the Ge-TeSe pseudo binary join led to the composition $Ge_{20}Te_{40}Se_{40}$, an unusual example of a material which forms very fine (~100Å) crystallites when cooled from the melt. The presence of these crystals was determined from X-ray diffraction patterns and could not be observed by the appearance in optical microscopy of a metallurgically polished and etched surface which was typical of a homogeneous glass. Crystallization on this scale suggests internal nucleation which has not been previously reported for bulk chalcogenide materials. This composition falls in the midst of the two-phase region with two T_g materials lying on either side along the Ge-TeSe join. Since $Ge_{20}Te_{40}Se_{40}$ lies along the $GeSe_2$-Te join, it is perhaps indicative of the most extreme case of phase separation if indeed, $GeSe_2$ is the separating phase. This composition could not be rendered amorphous using the spray cooling technique although vitreous samples with slightly higher (22%) and slightly lower (18%) Ge content could be prepared by spray cooling. This result supported the view that homogeneous nucleation of Te crystals was occurring during cooling. When samples prepared by r.f. sputtering were examined with the DSC to determine the low temperature phase glass transition (Tg_1) only Tx_1 was observed. X-ray analysis revealed these to be very fine Te crystals (~60Å). The thermal evolution of these internally nucleated crystals led directly to a detailed X-ray investigation including the study of kinetics of Te precipitation and particle growth as a function of annealing temperature.

A side-light of phase separation in glass forming systems is its close phenomenological association with "controlled" or "catalyzed" crystallization.[40] While glass forming liquids rarely can be supercooled sufficiently to reach $T^* \approx T_m/2$,[41] before reaching $T_g \approx \frac{2T_m}{3}$ where T^* is the temperature for homogeneous nucleation of crystals, the process of phase separation of a homogeneous liquid often leads to the situation where one or both liquid phases are sufficiently supercooled below the liquidus of the separated phase's composition that T^* is achieved and homogeneous nucleation can occur. This highly interesting effect lies at the heart of the Pyroceram technology[42] developed at Corning Glass Works in the 1950's and 1960's.

The phase separating process produces ideally dispersed and non-interacting droplets for a study of homogeneous nucleation since free surface nucleation can only affect a minor portion of the droplets involved. The observation of phase separation and the nucleation of tellurium crystallization on an ultra-fine scale for the composition $Ge_{20}Te_{40}Se_{40}$ appeared to be a unique example of such behavior in chalcogenide systems and was therefore deemed to be worthy of the detailed study of the kinetics of tellurium nucleation and crystallization which is described in this Section.

3.2 Qualitative X-ray and TEM Observations of Crystallization Behavior

Results of the X-ray diffraction data taken from a single substrate of sputtered $Ge_{20}Te_{40}Se_{40}$ at increasingly higher temperatures are shown in Figure 3.1 . X-ray diffraction traces of the substrate annealed at 125°C for 30 minutes revealed no evidence of crystallization. The Bragg reflections of hexagonal Te increased in height and sharpened in breadth at each annealing

Fig. 3.1

X-ray diffraction patterns of a 3.2 μ $Ge_{20}Te_{40}Se_{40}$ sputtered film after a series of 30 minute annealing cycles at the following temperatures: ---- as deposited; —·—·—125°C; ——— 150°C; - - - - - 175°C; ——— 225°C.

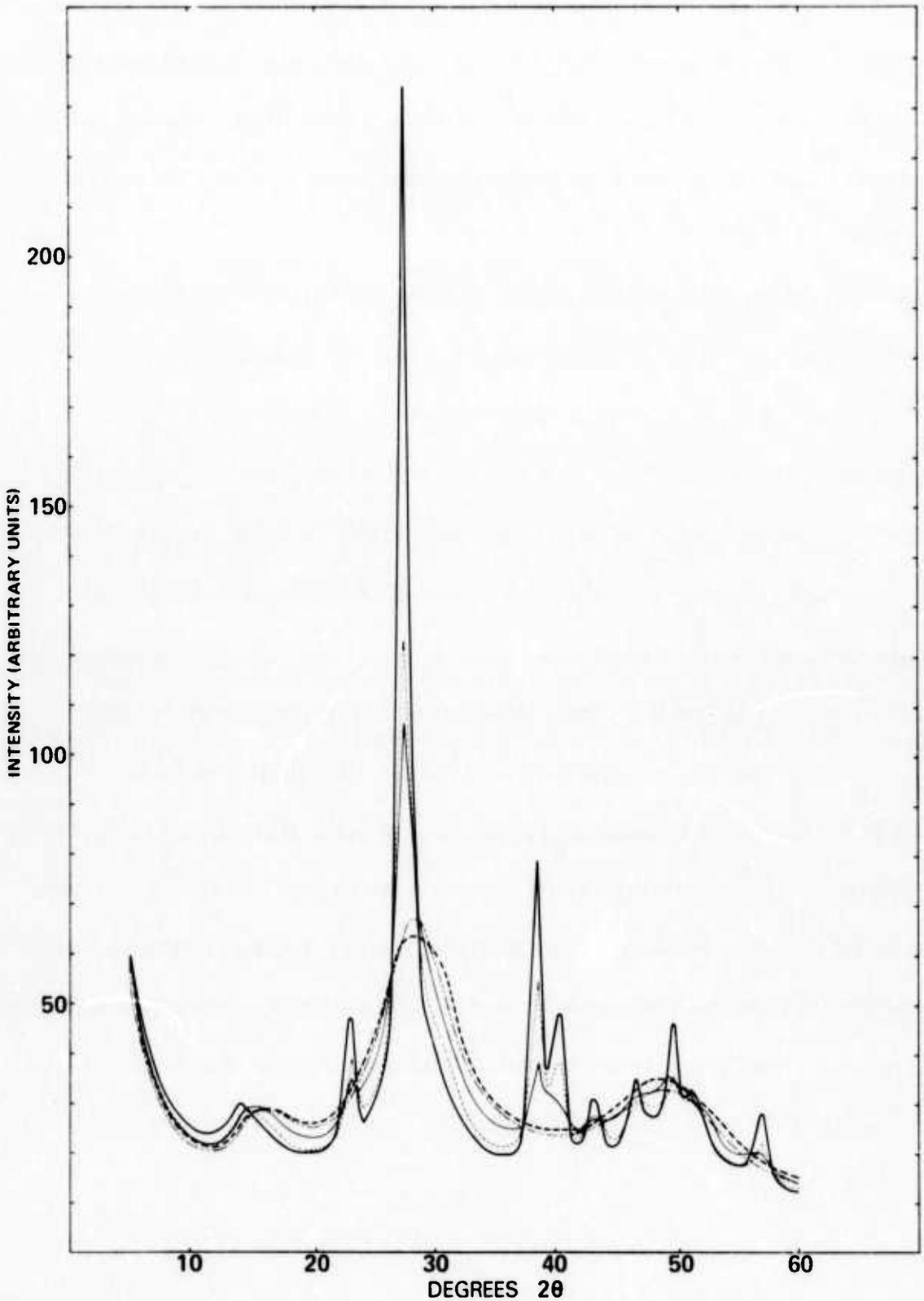
INTENSITY (ARBITRARY UNITS)
200
150
100
50
10
20
30
40
50
60
DEGREES 2θ

temperature from 150°C - 275°C. Only slight orientational effects appear to accompany crystal growth, with all reflections increasing continuously in intensity with progressively higher temperature annealing. Temperatures were kept considerably below the high temperature phase glass transition temperature of 340°C.

The extreme breadth of these Bragg reflections indicate a very small tellurium crystallite size. To confirm this result we sputtered a 300Å thin film of $Ge_{20}Se_{40}Te_{40}$ onto a carbon coated Ni TEM grid. We then annealed the substrate at 145°C for 30 minutes and examined it by TEM, obtaining the image shown in Figure 3.2a and the diffraction pattern shown in Figure 3.2b. The crystallite size calculated from the dimension of a typical diffracting (dark) particle in Figure 3.2a is 70Å. Since these particles are significantly smaller than the film thickness, they may have nucleated inside the film rather than at the film surface. As we shall see from the results to be presented in Section 3.3.2, this particle size compares favorably with the size of the coherently diffracting regions in the 3 - 5μm thick films crystallized at the same temperature and analyzed by X-ray diffraction. This agreement in crystallite size independent of film thickness provides a strong indication that the Te crystallites have indeed nucleated at many closely spaced points internal to the film itself.

Fig. 3.2

TEM photomicrograph and TED for ~ 500 Å $Ge_{20}Te_{40}Se_{40}$ film annealed at 145°C for 30 minutes.

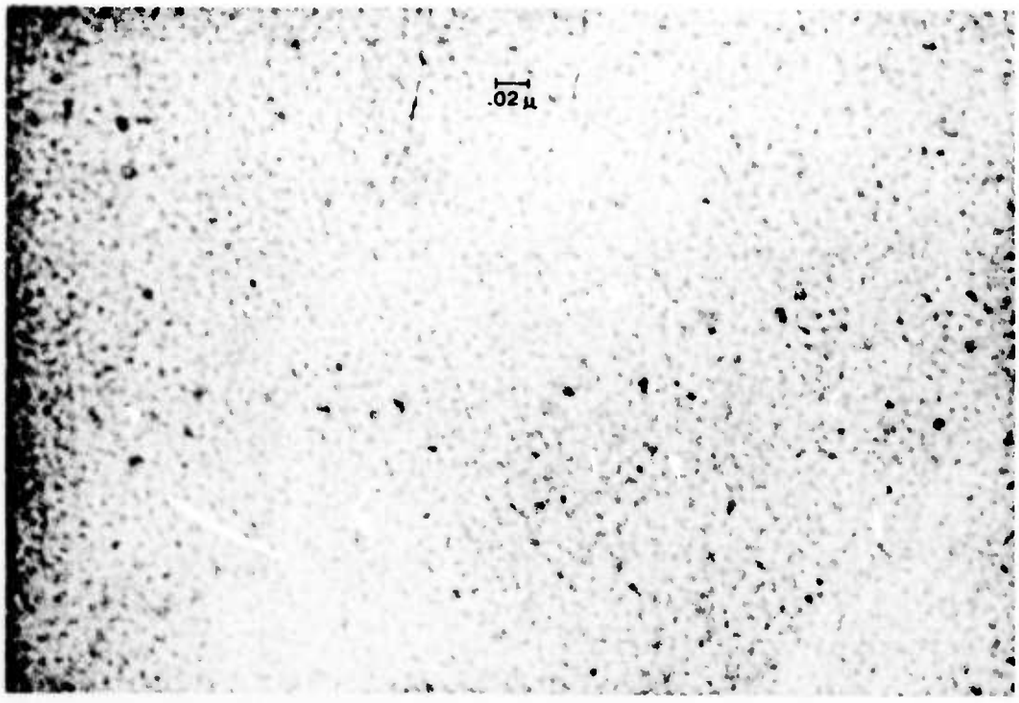

(a) TEM photograph of Ge_{20} Se_{40} Te_{40} annealed at 145°C for 30 minutes. Crystallite particle size is $\sim$ 68Å.

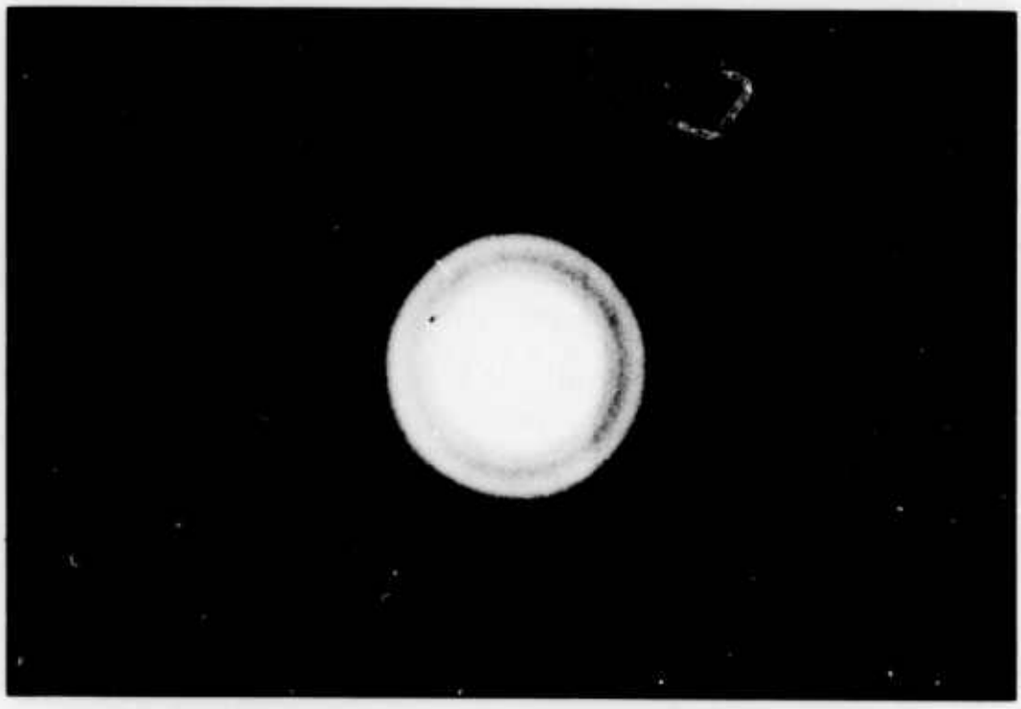

(b) Selected area diffraction from (a) showing crystalline Te pattern.

3.3 Study of Structural Evolution

3.3.1 Volume Fraction Calculations

From the X-ray diffraction data, it was possible to calculate volume fraction of crystals by measuring the area under the diffraction peaks; and to determine the crystallite size from measurements of peak breadths. To calculate the volume fraction of crystalline phases, the ratio of the integrated X-ray intensities for a given phase at a given temperature to the intensity from the corresponding reflection in the fully crystalline state is multiplied by the crystalline volume fractions in the fully crystalline state, i.e.

a) Volume fraction of Te crystals as a function of temperature =

$$\left[\frac{(\text{Te area})_T}{(\text{Te area})_{\text{fully crystalline}}} \right] \times 0.45$$

b) Volume fraction of $GeSe_2$ crystals as a function of temperature =

$$\left[\frac{(GeSe_2 \text{ area})_T}{(GeSe_2 \text{ area})_{\text{fully crystalline}}} \right] \times 0.55$$

c) Volume fraction of glass = 1 - (v.f. Te + v.f. $GeSe_2$) where the fully crystalline fractions are calculated as follows:

$$\text{Molecular volume} = \frac{\text{Molecular Weight}}{\text{Crystalline Density}} = \frac{cm^3}{g} \frac{g}{mole} = \frac{cm^3}{mole}$$

$$\rho_{Te} = 6.25 \text{ g/cm}^3$$

$$\rho_{GeSe_2} = 4.61 \text{ g/cm}^3$$

$$\text{Molar volume } Te_2 = 2\left(\frac{1}{6.25}\right)(127.60) = 40.84 \text{ cm}^3\text{/mole}$$

Molecular weight of $GeSe_2$

$= 75.59 + (78.96)2$

$= 230.49$ g/mole

Molar volume $GeSe_2$

$= \frac{230.49}{4.68}$

$= 49.26\ cm^3/mole$

Total molar volume = volume $GeSe_2$ + volume Te_2

$= 40.84 + 49.26 = 90.10\ cm^3$

Volume fraction:

$$Te = \frac{40.84}{90.10} = 45.3\%$$

$$GeSe_2 = \frac{49.26}{90.10} = 54.7\%$$

3.3.2 Particle Size Calculations

In addition to volume fraction calculations, it is possible to determine average particle size of crystalline phases from X-ray diffraction data. The widths of various Bragg reflections at one half maximum intensity were measured as a function of annealing temperature. The crystalline particle size was calculated by use of the Scherrer formula:

$$t = \frac{0.94\lambda}{B\cos\theta_B}$$

where: t = particle size diameter in Å

λ = wavelength of X-ray in Å

θ_B = angle of incidence

B = broadening of diffraction line in radians.

To determine B, the instrumental broadening must be subtracted from the measured broadening by some appropriate method; the method of Warren[43] was used in this study. To determine the broadening due to particle size effect alone, the instrumental broadening B_s, was taken as the Bragg reflection breadth of a silicon powder standard extrapolated as a function of 2θ within the region of interest. According to Warren, the calculated peak breadth B, is related to the measured breadth, B_m, by:

$$B^2 = B_m^2 - B_s^2 .$$

This method of crystallite size determination is shown in the following example for a $Te_{(101)}$ reflection annealed at 250°C for 60 minutes. The base line drawn beneath the Bragg reflection is taken to be the lower limit or base intensity while the peak is taken as the upper limit or maximum intensity.

Maximum intensity = 98%

Base intensity = 14%

Intensity at 1/2 maximum = 56%

$\Delta 2\theta_{(101)} = 1.075^{\circ}2\theta$ at $27.6^{\circ}2\theta$

$\Delta 2\theta_{(hkl)}$ from Si standard at $27.6^{\circ}2\theta = 0.156^{\circ}2\theta$

$$B^2 = B_m^2 - B_s^2$$

$$B^2 = \left[(1.075^\circ 2\theta)(0.01745 \text{ rad/deg})\right]^2 - \left[(0.156^\circ 2\theta)(0.01745 \text{ rad/deg})\right]^2$$

$$B = 0.01856 \text{ rad}$$

$$t = \frac{0.94\lambda}{B\cos\theta}$$

$$= \frac{(0.94)(1.542\text{Å})}{(0.01856)(\cos 13.8^\circ)}$$

$$= 80.4\text{Å}$$

This is in good agreement with the upper limit of the $Ge_{20}Te_{40}Se_{40}$ tie line in Figure 3.8.

3.3.3 Integrated Bragg Peak Intensity Results

X-ray diffraction of bulk thin film of $Ge_{20}Se_{40}Te_{40}$ and of sputtered samples indicated that Te crystallites are not nucleated on the surface but are internally nucleated with random orientations. These observations were confirmed by TEM observations as described in Section 3.2. To monitor the nucleation, growth, and ripening of these Te crystals, a quantitative X-ray study was carried out with a series of amorphous sputtered

film samples held at progressively higher annealing temperatures. The integrated intensities and breadths of the Te (100), (101), (003) and $GeSe_2$ (111), (103) Bragg reflections were chosen to determine particle size, shape and volume fraction during thermal crystallization. Table 3.1 gives the relative integrated X-ray intensities of these peaks related to those of the fully crystalline state at 375°C.

A measurable increase in Te diffraction intensity accompanies the precipitation of $GeSe_2$ at 375°C. The volume fraction as a function of annealing temperature is taken from the average of individual (hkl) reflections. The comparison of the A.S.T.M.[52] standard powder pattern reflection intensities for Te and $GeSe_2$ to the measured X-ray intensities verifies the random orientation of the crystallites present.

The volume fraction of each phase is shown in Figure 3.3 as a function of annealing temperature. It can be seen that Te reaches a saturation volume fraction of roughly 0.34 between 175°C and 275°C until nucleation of $GeSe_2$ crystals occurs. The increase in the volume fraction of Te crystals upon nucleation and growth of $GeSe_2$ crystals can now quantitatively be evaluated and provides a measure of the Te content of the high T_g glassy phase of $Ge_{20}Se_{40}Te_{40}$.

A rough calculation for the atomic percent of Te in ghe $GeSe_2$-rich amorphous phase of $Ge_{20}Te_{40}Se_{40}$ at 350°C can be made from the volume fraction data before and after $GeSe_2$ crystallization shown in Figure 3.3. The amount of Te in the $GeSe_2$-rich phase is simply the difference between the lower saturation level of Te crystallites between 200 and 350°C and the

TABLE 3.1

X-RAY DATA FOR THERMAL CRYSTALLIZATION OF SPUTTERED AMORPHOUS $Ge_{20}Te_{40}Se_{40}$ FILMS: INTENSITIES

Annealing Temperature (°C)	Integrated X-Ray Intensities (Arbitrary Units)					Relative Intensities				
	Te			$GeSe_2$		Te, (101) = 100			$GeSe_2$, (111) = 100	
	(100)	(101)	(003)	(111)	(103)	(100)	(101)	(003)	(111)	(103)
$Ge_{20}Se_{40}Te_{40}$										
150	1.58	12.7	-	0	0	12.4	100	-	0	0
175	3.22	25.2	1.47	0	0	12.8	100	5.82	0	0
225	4.88	36.9	2.21	0	0	13.2	100	6.00	0	0
250	4.00	36.0	3.00	0	0	11.1	100	8.31	0	0
275	5.46	37.1	3.21	0	0	14.8	100	8.67	0	0
310	3.99	39.5	2.95	0	0	10.1	100	7.46	0	0
340	5.23	34.3	2.82	0	0	15.2	100	8.20	0	0
375	6.35	49.1	4.78	8.02	4.59	12.9	100	9.70	100	57.2
Te* (Crystalline Powder)						20	100	8.0	100	40
$GeSe_2$** (Crystalline Powder)										

Fig. 3.3

Volume fraction of crystallization products for $Ge_{20}Te_{40}Se_{40}$ films as a function of annealing temperature.

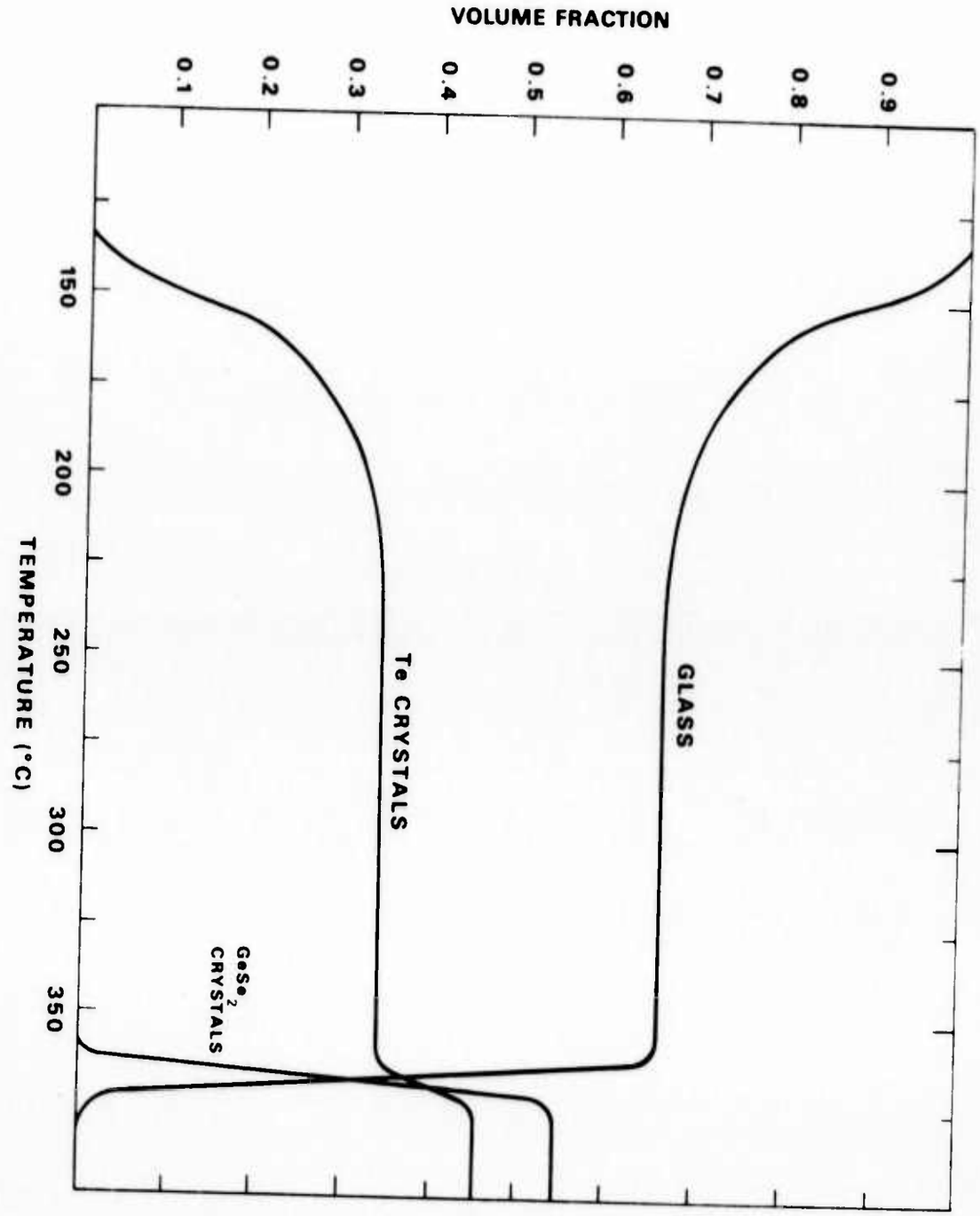
VOLUME FRACTION
0.1
0.2
0.3
0.4
0.5
0.6
0.7
0.8
0.9
150
200
250
300
350
TEMPERATURE (°C)
GLASS
Te CRYSTALS
GeSe2 CRYSTALS

upper saturation level of Te crystals nucleated by crystallization of $GeSe_2$ at 375°C. This calculation is as follows:

$$\text{Atom fraction of crystalline Te at } 350^{\circ}C$$

$$= \left(\begin{array}{l}\text{atom fraction} \\ \text{Te in } Ge_{20}Te_{40}Se_{40}\end{array}\right)\left(\frac{\text{volume fraction of Te crystallized}}{\begin{array}{l}\text{volume fraction of Te in} \\ Ge_{20}Te_{40}Se_{40}\end{array}}\right)$$

$$= (0.4)\left(\frac{0.34}{0.45}\right) = 0.30$$

By difference, the composition of the residual glass phase at 350°C contains 0.4 - 0.3 = 0.1 gm atoms of Te, i.e., $Ge_{20}Te_{10}Se_{40}$, corresponding to $Ge_{28.6}Te_{14.3}Se_{57.1}$ when normalized to 100 atomic percent. This value is in close agreement with the composition of the high T_g $GeSe_2$-rich glass calculated by the tie-line method.

3.3.4 Particle Size Evolution vs. Annealing Temperature

The nucleation growth of Te and $GeSe_2$ crystallites as a function of annealing temperature from particle size determinations of peak breadths are shown in Table 3.2. By direct comparison of the particle size for Bragg reflections in Te and $GeSe_2$ it is noted that no strong shape assymetry accompanies primary crystallization or grain coarsening. The particle sizes corresponding to these reflections are plotted in Figure 3.4 as a function of annealing temperature. Very rapid growth of the Te crystallites occurs between 135°C to 150°C in the same range where the Te volume fraction is increasing rapidly. Between 200°C and 350°C the particle size increases slightly while, as we have seen in Figure 3.3, the crystalline Te volume fraction stays roughly constant. $GeSe_2$ nucleates at 375°C leading to a rapid increase in Te particle size.

TABLE 3.2

X-RAY DATA FOR THERMAL CRYSTALLIZATION OF SPUTTERED AMORPHOUS $Ge_{20}Te_{40}Se_{40}$ FILMS: INTENSITIES

Annealing Temperature (°C)	Integrated X-Ray Intensities (Arbitrary Units)					Relative Intensities				
	Te			$GeSe_2$		Te, (101) = 100			$GeSe_2$, (111) = 100	
	(100)	(101)	(003)	(111)	(103)	(100)	(101)	(003)	(111)	(103)
$Ge_{20}Se_{40}Te_{40}$										
150	1.58	12.7	-	0	0	12.4	100	-	0	0
175	3.22	25.2	1.47	0	0	12.8	100	5.82	0	0
225	4.88	36.9	2.21	0	0	13.2	100	6.00	0	0
250	4.00	36.0	3.00	0	0	11.1	100	8.31	0	0
275	5.46	37.1	3.21	0	0	14.8	100	8.67	0	0
310	3.99	39.5	2.95	0	0	10.1	100	7.46	0	0
340	5.23	34.3	2.82	0	0	15.2	100	8.20	0	0
375	6.35	49.1	4.78	8.02	4.59	12.9	100	9.70	100	57.2
Te* (Crystalline Powder)						20	100	8.0	100	40
$GeSe_2$** (Crystalline Powder)										

TABLE 3.2 CONT.

X-RAY DATA FOR THERMAL CRYSTALLIZATION OF SPUTTERED AMORPHOUS $Ge_{20}Te_{40}Se_{40}$ FILMS: INTENSITIES

Annealing Temperature (°C)	Relative Integrated X-Ray Intensities (hkl) 375°C = 100%					Averaged Integrated X-Ray Intensities (hkl) 375°C = 100%		Volume Fractions Calculated from Averaged Integrated X-Ray Intensities and Crystal Densities		
	Te			$GeSe_2$						
	(100)	(101)	(003)	(111)	(103)	Te	$GeSe_2$	Te	$GeSe_2$	Glass 1-(Te+$GeSe_2$)
150	24.9	25.9	-	0	0	25.4	0	.117	0	.893
175	50.7	-	30.8	0	0	40.8	0	.188	0	.812
225	76.9	75.0	46.2	0	0	66.0	0	.304	0	.696
250	63.0	73.3	62.9	0	0	66.4	0	.305	0	.695
275	88.2	75.4	67.3	0	0	77.0	0	.354	0	.646
310	62.8	80.5	61.7	0	0	68.3	0	.314	0	.686
340	82.4	69.8	59.0	0	0	70.4	0	.324	0	.676
375	100	100	100	100	100	100	100	.460	.54	0

* ASTM File #4-554, ** ASTM File #16-080

Fig. 3.4

Crystallite size as a function of annealing temperature for $Ge_{20}Se_{40}Te_{40}$ films.

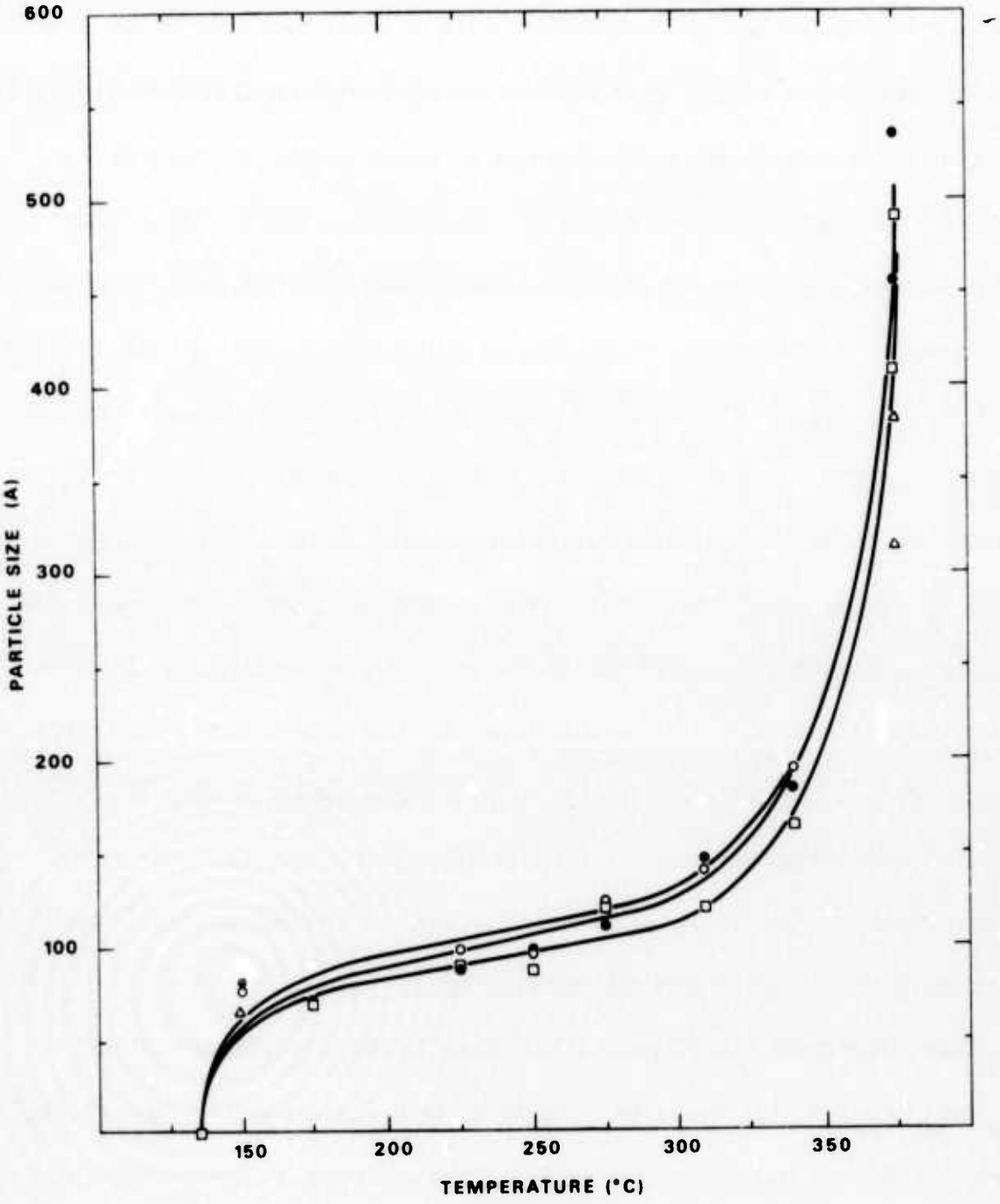
600
500
400
300
200
100
PARTICLE SIZE (A)
150
200
250
300
350
TEMPERATURE (°C)

3.4 Discussion and Conclusions

To understand the rather unique crystallization behavior of $Ge_{20}Se_{40}Te_{40}$, one must recall Luo's[44] unsuccessful efforts to splat cool pure Te liquid to form the amorphous state. Even holding the splat-receiving surface at liquid nitrogen or liquid helium temperature had no effect on the structure of the resulting crystalline splatted products. Of course no pure metallic liquid has been splatted to form an amorphous solid, and liquid Te has many metallic properties.[45] Furthermore, sputtered and evaporated amorphous tellurium films crystallize in the vicinity of $0^{\circ}C$,[46] and, if we take this temperature as an approximation of T_g, then $T_m/T_g \approx 0.4$. Because typical values of $T^*/T_g \approx 0.5$, where T^* is the critical temperature for homogeneous nucleation, T^* lies above T_g, and a liquid being cooled from T_m toward T_g would be expected to nucleate and crystallize at T^* unless the viscosity of the liquid T^* is sufficiently high to inhibit the nucleation rate. Similar effects would be expected in super cooled Te-rich alloy liquids whether obtained by cooling of a homogeneous liquid phase or by separation of a Te-rich liquid phase during the cooling of some other liquid alloy which undergoes phase separation upon crossing into a region of liquid immiscibility.

This latter possibility apparently occurs during the cooling of liquid $Ge_{20}Se_{40}Te_{40}$, which separates a liquid Te-rich phase which rapidly crystallizes. Analogous behavior presumably occurs as initially homogeneous sputtered amorphous films of $Ge_{20}Se_{40}Te_{40}$ are heated above about $125^{\circ}C$, and Te crystals are formed on a very fine scale (~50Å or less) within the film.

The agreement between particle size and volume fraction measurements on 400Å thick TEM samples and 4μm thick X-ray diffraction samples annealed at the same temperature indicates that the crystals form at a uniform rate throughout the film thickness, and are not preferentially nucleated at the surface. This result contrasts with the observations of Moss and deNeufville [53] who observed surface nucleation of Te crystals on sputtered films of $Te_{83}Ge_{17}$ and $Te_{81}Ge_{15}S_2Sb_2$ when these films were annealed in the vicinity of T_g. In that case transmission electron diffraction (TED) and reflection electron diffraction (RED) indicated Te crystals at a much lower annealing temperature than X-ray diffraction, proving the role of surface nucleation. Indeed, chalcogenide glasses in general have been shown to nucleate crystals mostly at free surfaces, and the present observations represent an unusual contrast to this normal result.

In order to understand the uniqueness of the crystallization behavior of $Ge_{20}Se_{40}Te_{40}$ in comparison to alloys containing slightly more or slightly less Ge (which can be sprayed to form two-phase glasses), it is useful to further examine qualitatively the compositional dependence of T_g, T^* and T_m in the ternary Ge-Se-Te system in the vicinity of Te. In Figure 3 we show such a schematic plot for homogeneous Te-rich alloys which indicates that T^* decreases and T_g increases as the Ge and Se content of the alloy increases. As T^* approaches T_g, a new effect [46] enters into the theory of homogeneous nucleation, the rate of aggregation of unstable equilibrium clusters due to viscosity effects. For T^* near T_g this effect rapidly reduces the nucleation rate, rendering invalid the correlation of T^* with T_m which we have assumed. As the Te content of the

Fig. 3.5

Schematic representation of T_m, liquidus temperature, T_g, glass transition temperature, and T^* ($T^* = T_m/2$), homogeneous nucleation temperature, all versus Ge+Se content in Te-Ge+Se system.

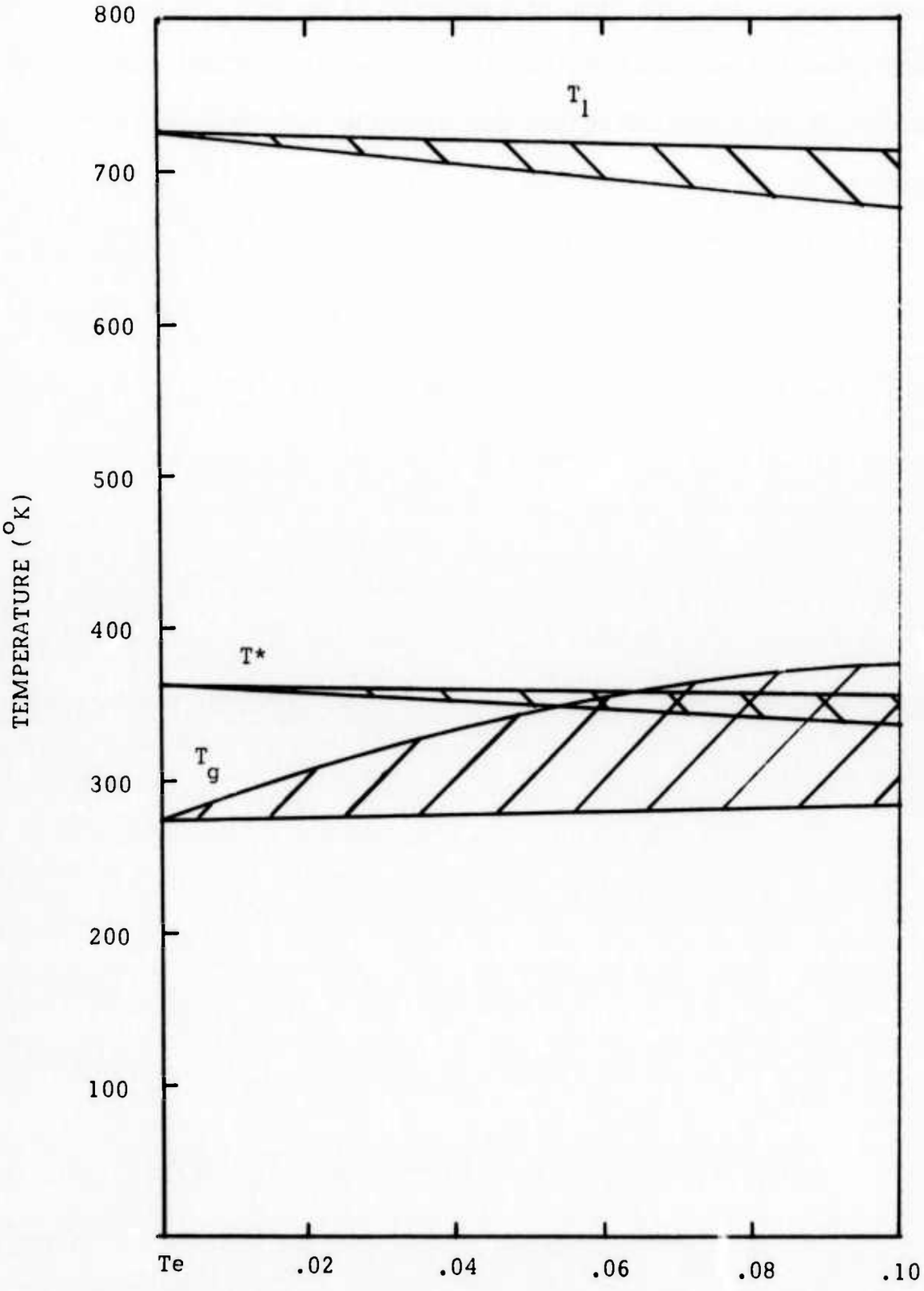
800
700
600
500
400
300
200
100
T_l
T*
T_g
TEMPERATURE (^oK)
Te
.02
.04
.06
.08
.10
ATOM FRACTION Se, Ge

Te-rich amorphous phase in the immiscibility portion of the $GeSe_2$-$GeTe_2$-Se-Te sub-system is also a sensitive function of the average composition of the phase-separating alloy, it is thus understandable that the probability of homogeneous nucleation of Te crystals is itself a very sensitive function of average alloy composition.

4. ELECTRICAL AND OPTICAL PROPERTIES OF AMORPHOUS PHASES IN THE Ge-Se-Te SYSTEM

4.1 Introduction

In other papers we have described optical, electrical, and thermoelectric properties of the Ge-Te[47] and $GeTe_2$-$GeSe_2$[48] binaries in detail. Here we will summarize these properties for sputtered films in the entire Ge-Te-Se ternary system. The $GeTe_2$-$GeSe_2$ pseudobinary line in this system is particularly interesting because it represents the line of stoichiometric compositions for four-fold coordinated Ge and two-fold coordinated chalcogen atoms. That is, it is possible to obtain chemical ordering along this line in the sense that all bonds are between Ge and chalcogen atoms. Binaries in the other direction, such as the Ge-Te and Ge-Se binaries, are also interesting, because striking changes in properties with composition can result as atoms from two different columns of the periodic table are mixed.

4.2 Summary of Electrical and Optical Properties

Here we summarize properties both for films as-deposited on room temperature substrates and for annealed films. For materials which have a T_g the films were heated to a temperature near T_g where the optical and electrical properties were independent of annealing temperature (see Fig. 2.13 of the 3rd Semiannual Technical Report). For the Ge-rich materials which have no T_g, choice of an annealing temperature is somewhat arbitrary, although it is limited by the crystallization temperature. Also, the crystallization temperature

itself is somewhat ambiguous since the crystallization rate is a thermally activated process. Figure 4.1 shows glass transition temperatures and crystallization temperatures for the Ge-Te and Ge-Se binaries. The glass transition temperature was determined in a scanning calorimeter at a rate of 20 deg/min. Crystallization temperatures are approximate temperatures obtained on a convenient laboratory time scale (of the order of seconds or minutes). For the physical properties ascribed to an annealed state in this discussion, we chose annealing temperatures that increased with increasing Ge-content, as indicated in Fig. 4.1.

Figure 4.2 shows the optical gap E_{O4} (defined as the photon energy at which the absorption coefficient is $10^4 cm^{-1}$) vs. fraction of germanium for the Ge-Te, Ge-Se, and Ge- $Te_{0.5}Se_{0.5}$) binaries. Just as a strong peak at $GeTe_2$ was found for annealed materials in the Ge-Te binary, so also are such peaks found in the Ge-Se and Ge-($Te_{0.5}Se_{0.5}$) binaries. Unannealed materials have smaller optical gaps and show the same general qualitative bahavior as the annealed materials, except that the peaks near the stoichiometric compositions are not sharp. On the Ge-rich half of the binary, all three binaries have optical gaps which lie below a linear line connecting the endpoints; this will be discussed for the Ge-Te binary in the Final Technical Report for this contract.

The conductivity at room temperature is shown for the same binaries in Fig. 4.3. This plot is similar to an inverted optical gap plot, and reflects the fact that the major variations of conductivity with composition

Fig. 4.1

Glass transition temperature T_g, crystallization temperature T_x, and the annealing temperature employed in this work for the germanium-rich portion of the Ge-Te, Ge-Se, and Ge-$(Se_{0.5}Te_{0.5})$ binaries. Transition temperatures were determined in a calorimeter scanned at a rate of 20 deg/min.

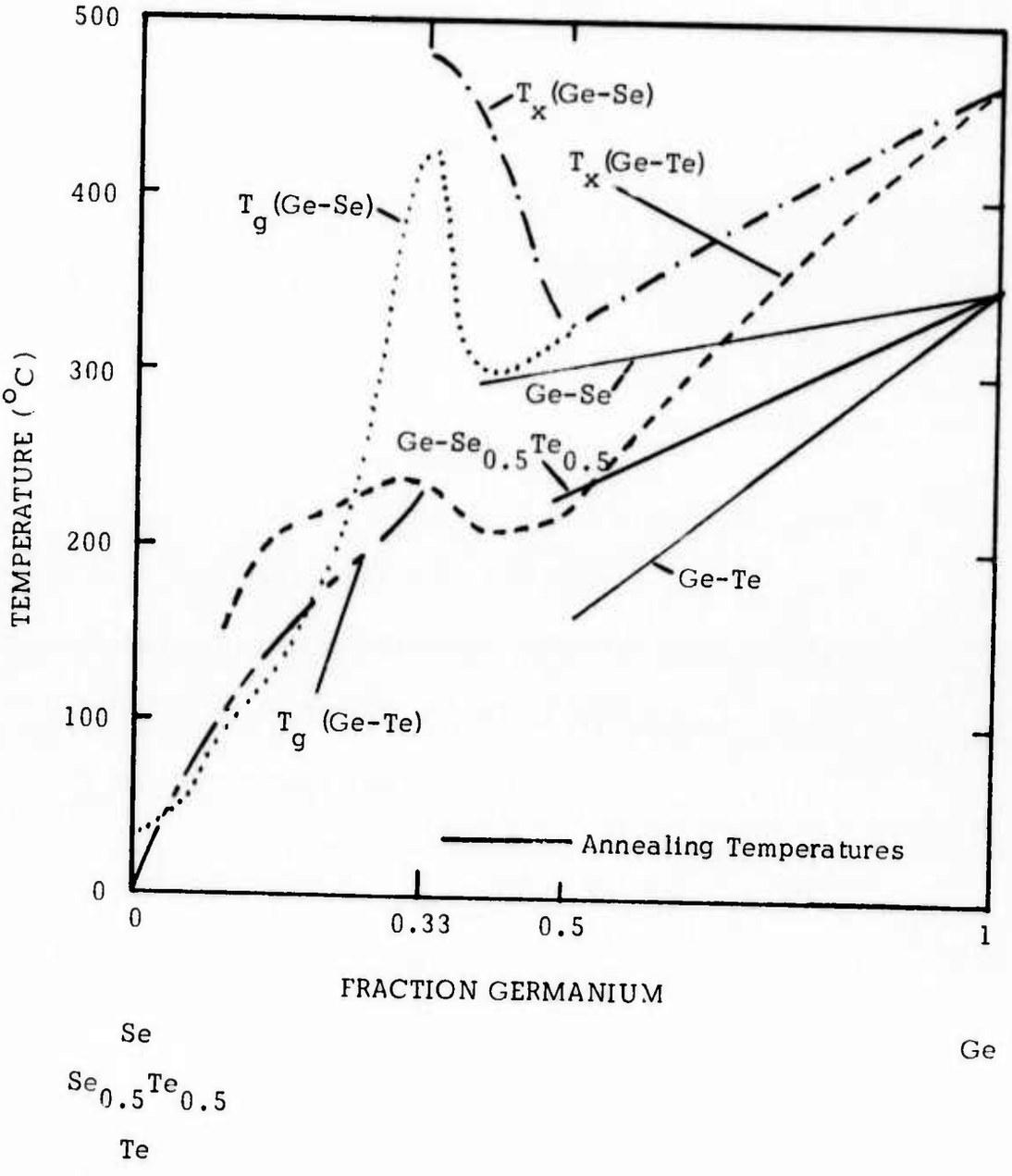
500
400
300
200
100
0
TEMPERATURE (°C)
T_x (Ge-Se)
T_x (Ge-Te)
T_g (Ge-Se)
Ge-Se
$Ge\text{-}Se_{0.5}Te_{0.5}$
Ge-Te
T_g (Ge-Te)
Annealing Temperatures
0
0.33
0.5
1
FRACTION GERMANIUM
Se
$Se_{0.5}Te_{0.5}$
Te
Ge

Fig. 4.2

Optical gap E_{O4} (photon energy at which the absorption coefficient is $10^4 cm^{-1}$) vs. fraction of germanium for annealed films in the Ge-Se, Ge-$(Se_{0.5}Te_{0.5})$, and Ge-Te binaries. The discontinuity in the line for the Ge-$(Se_{0.5}Te_{0.5})$ system corresponds to the phase separating region.

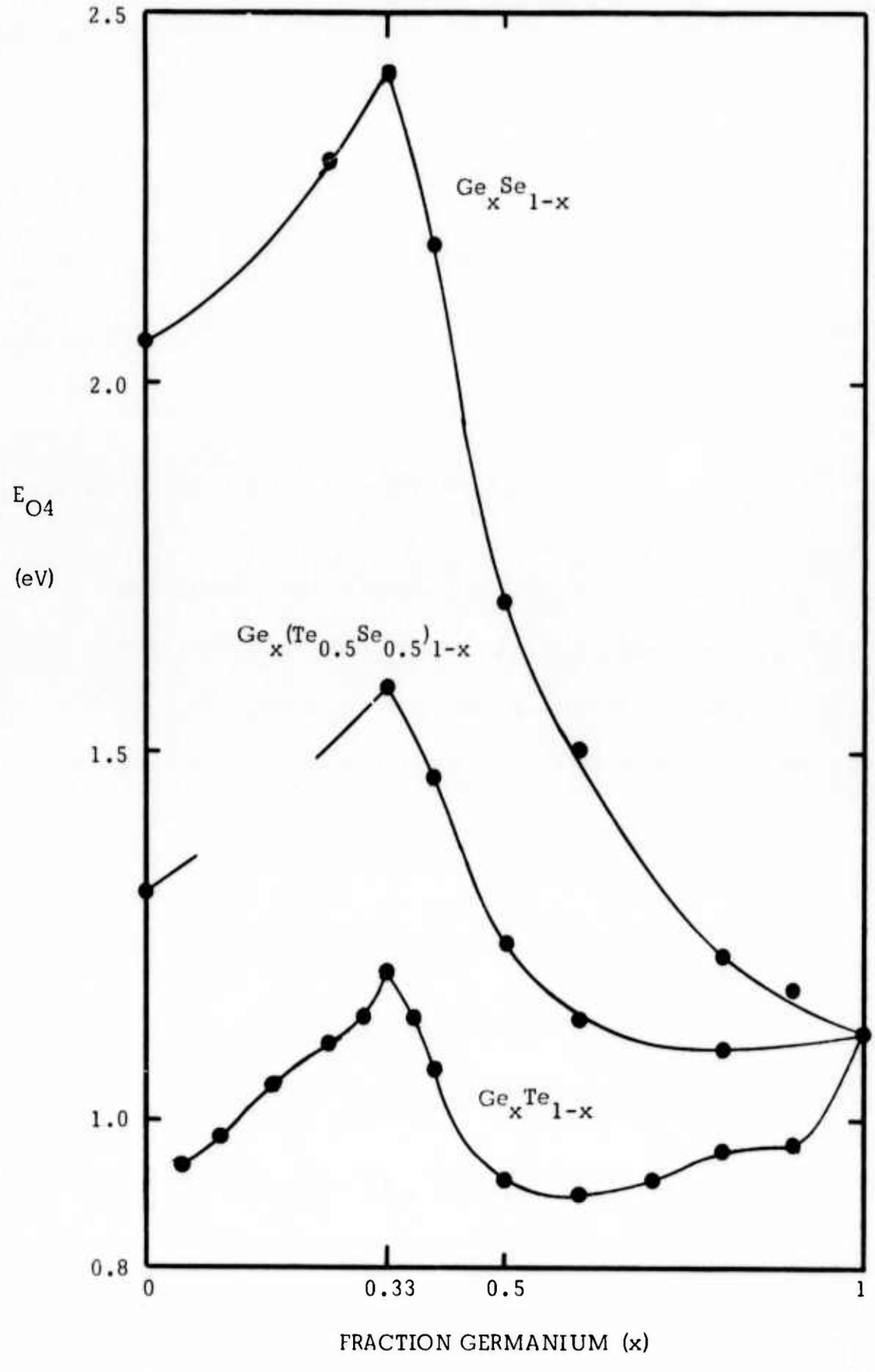
2.5
2.0
1.5
1.0
0.8
E_{O4}
(eV)
Ge_xSe_{1-x}
$Ge_x(Te_{0.5}Se_{0.5})_{1-x}$
Ge_xTe_{1-x}
0
0.33
0.5
1
FRACTION GERMANIUM (x)
X
Ge

Fig. 4.3

Electrical conductivity at 25°C vs. fraction of germanium for annealed films in the Ge-Se, Ge-$(Se_{0.5}Te_{0.5})$, and Ge-Te binaries. The discontinuity in the line for the Ge-$(Se_{0.5}Te_{0.5})$ system corresponds to the phase separating region.

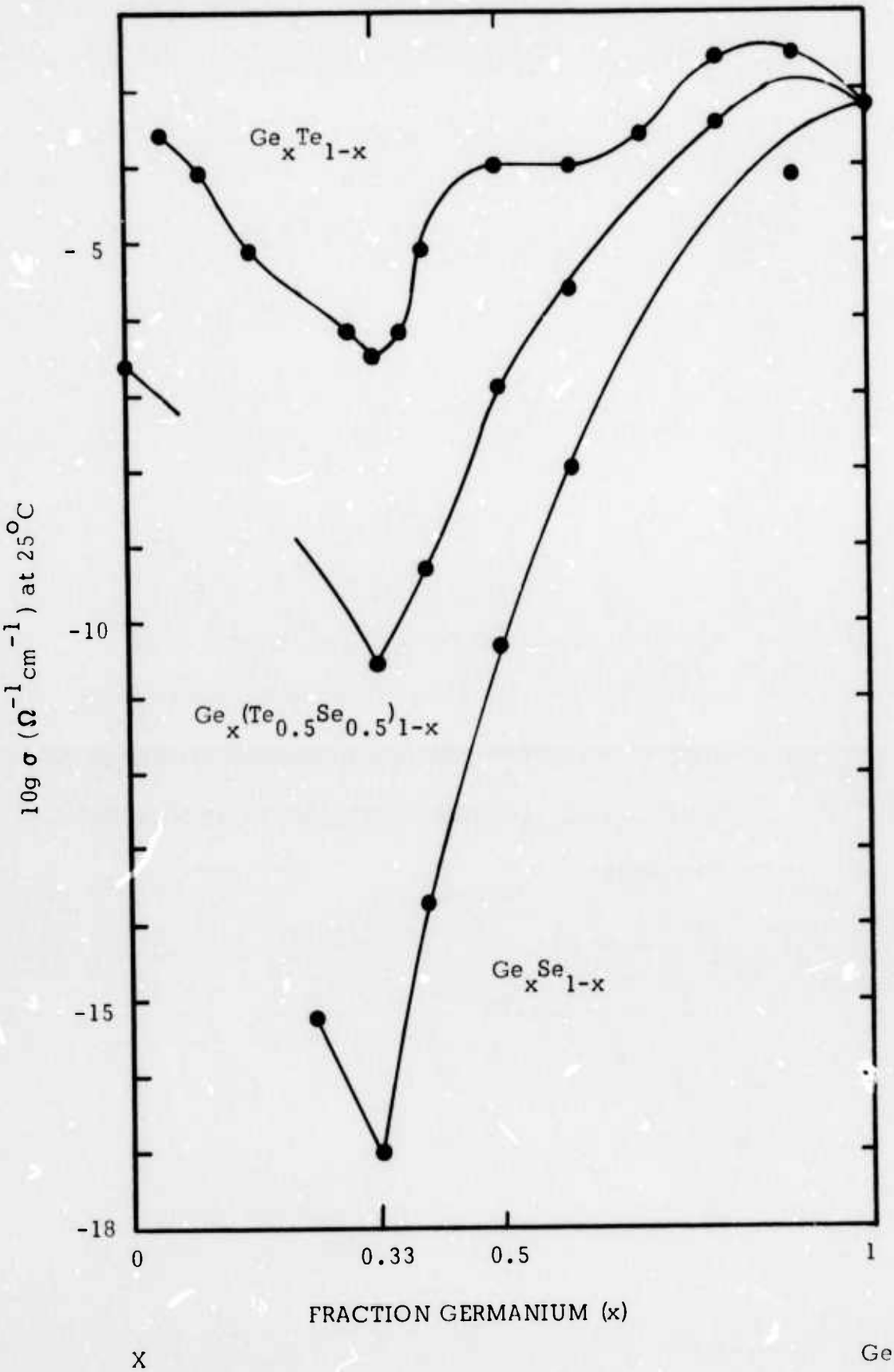
Ge_xTe_{1-x}
$Ge_x(Te_{0.5}Se_{0.5})_{1-x}$
Ge_xSe_{1-x}
- 5
-10
-15
-18
0
0.33
0.5
1
$10g\ \sigma\ (\Omega^{-1}cm^{-1})$ at 25°C
FRACTION GERMANIUM (x)
X
Ge

are dominated by the variations of the gap.

4.3 Discussion

The extrema in various physical properties at $GeTe_2$, GeTeSe, and $GeSe_2$ are associated with the structure, the bond strengths, and the ionic components of the bonds for the various alloys. This was discussed by Rockstad and deNeufville for the Ge-Te binary.[47] Let $X_2 = Te_2$, Se_2, or TeSe. Based on the observed extrema we infer the following. The structure of annealed amorphous GeX_2 is a fully cross-linked covalently bonded structure, with Ge in 4-fold coordination and Se and/or Te in 2-fold coordination, in analogy with vitreous silica. The only bonds in this structure are bonds between Ge and chalcogen atoms. Compositions to either side of GeX_2 have excess Ge or excess chalcogen with respect to GeX_2, and hence must have Ge-Ge or X-X bonds as well as Ge-X bonds. Because of the ionic component of the Ge-X bonds, the effective bond strength is greater for GeX_2 than for other compositions, giving rise to the maxima in the optical gaps and to extrema in other physical properties.

Based on the electrical, thermoelectric, and optical data, we believe that the dominant room temperature dc conduction in the Ge-rich portion of the ternary takes place near the Fermi level by hopping in localized states. Addition of up to about 10% of Te and/or Se adds more localized states in the gap, which results in a larger hopping conductivity in the case of Te additions.

For more than 30% of Te and/or Se, the dominant conduction takes place in either the valence or conduction band. For these alloys with more than 30%

Te or Se the densities of localized states in the gap between the valence and conduction bands are considerably smaller than the density of localized states for Ge. This observation is apparently the result of the bonding flexibility introduced by tellurium or selenium as opposed to the inflexible tetrahedral bonds of germanium.

Although the germanium tellurides were found to be p-type in both the unannealed and annealed states, except for greater than 60% Ge-contents, we found that replacement of Te by Se brought about a tendency toward negative thermopowers (S) and negative slopes of the S vs. 1/T plots for the annealed states. The unannealed states of these materials were nevertheless p-type.

Figure 4.4(a) and (b) shows the p-type and n-type regions of the ternary for unannealed and annealed films. Compositions included in this study are indicated in the figures. It is interesting that p-type behavior persists to larger Se:Te ratios along the GeTe-GeSe pseudobinary than along the $GeTe_2$-$GeSe_2$ pseudobinary. Note also the sizable composition range where unannealed alloys are p-type but annealed alloys are n-type. Iso-resistivity lines for the ternary are shown in Figure 4.5(a) and (b). For annealed alloys there is a sharp peak in resistivity along the $GeTe_2$-$GeSe_2$ pseudobinary line and a valley centering near $Ge_{90}Te_{10}$. The resistivities in the vicinity of $GeSe_2$ and Se have a relatively high degree of uncertainty both because of difficulty in measuring them and because, for such high resistivity materials, the sample resistances are very sensitive to impurities and contacts. Also,

Fig. 4.4

P- and n-type regions for sputtered amorphous films in the Ge-Se-Te ternary.

(a) Unannealed films deposited on substrate held near 25°C.

(b) Annealed films

The regions in the vicinity of selenium are undetermined.

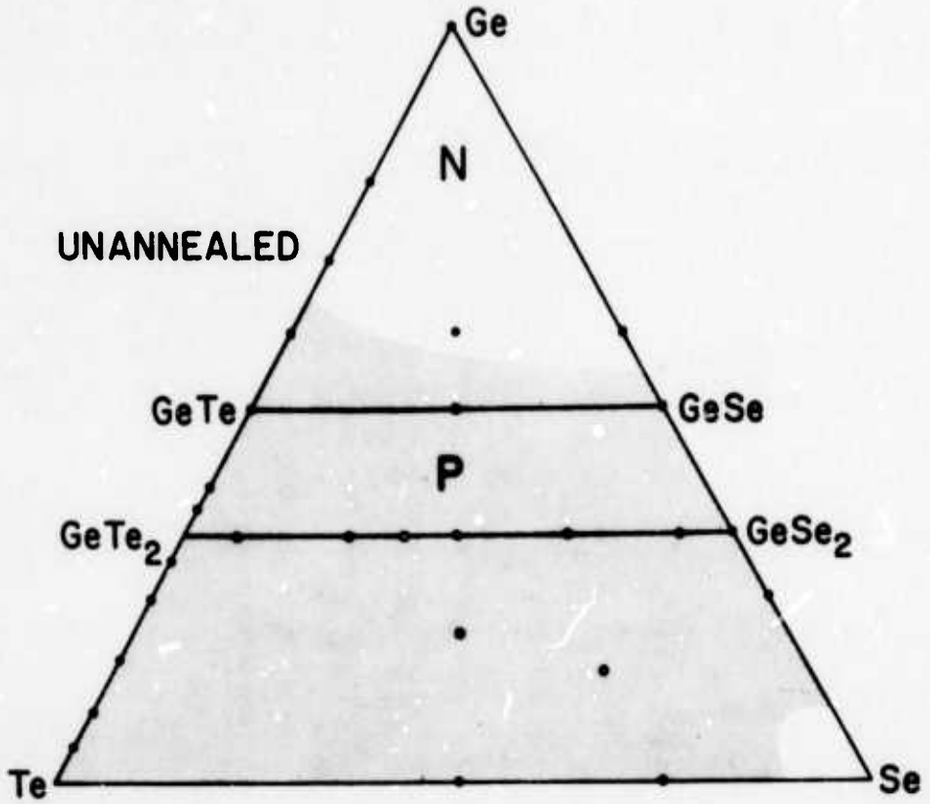
Ge
N
UNANNEALED
GeTe
GeSe
P
GeTe2
GeSe2
Te
Se

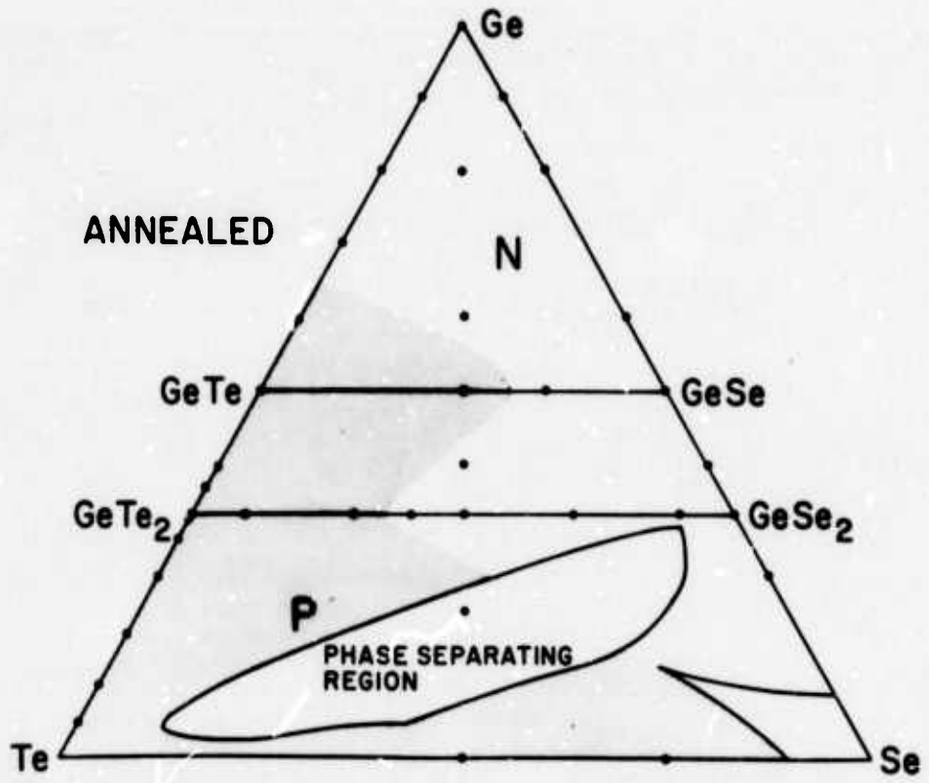
Ge
ANNEALED
N
GeTe
GeSe
GeTe2
GeSe2
P
PHASE SEPARATING
REGION
Te
Se

Fig. 4.5

Isoresistivity lines for sputtered amorphous films in the Ge-Se-Te ternary.

(a) Unannealed films.

(b) Annealed films.

Broken lines for high resitivity materials indicate materials whose resistivities have uncertainties as high as one to three decades, as discussed in the text.

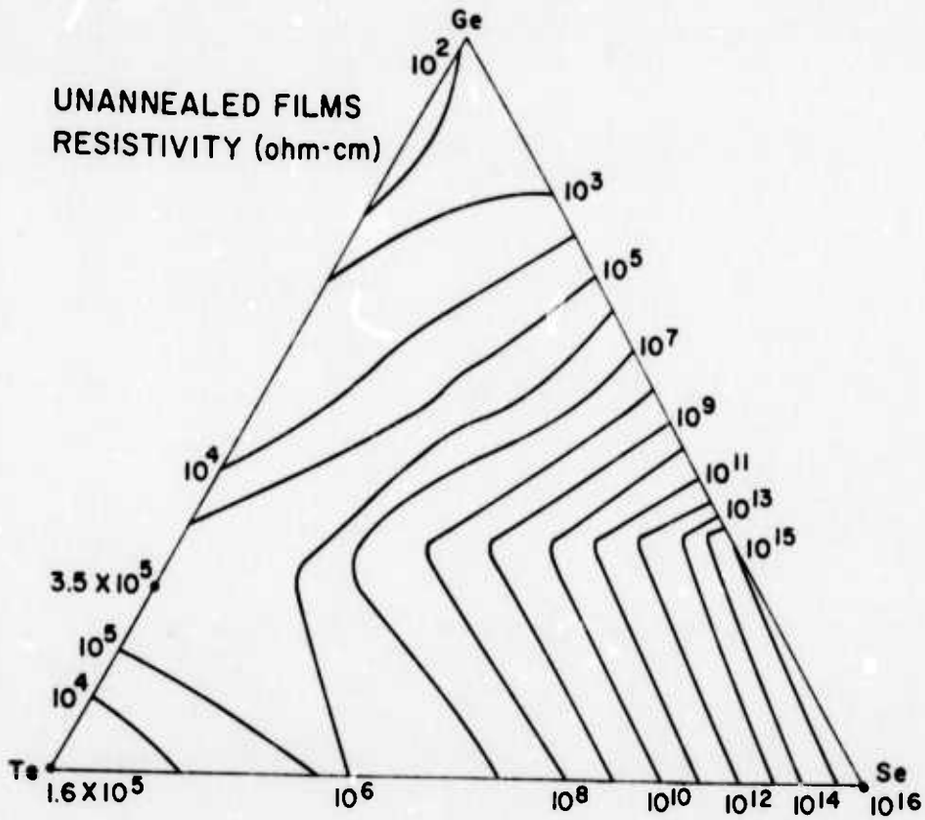
UNANNEALED FILMS
RESISTIVITY (ohm-cm)
Ge
Te
Se
10^2
10^3
10^4
10^5
10^7
10^9
10^{11}
10^{13}
10^{15}
3.5×10^5
10^5
10^4
1.6×10^5
10^6
10^8
10^{10}
10^{12}
10^{14}
10^{16}

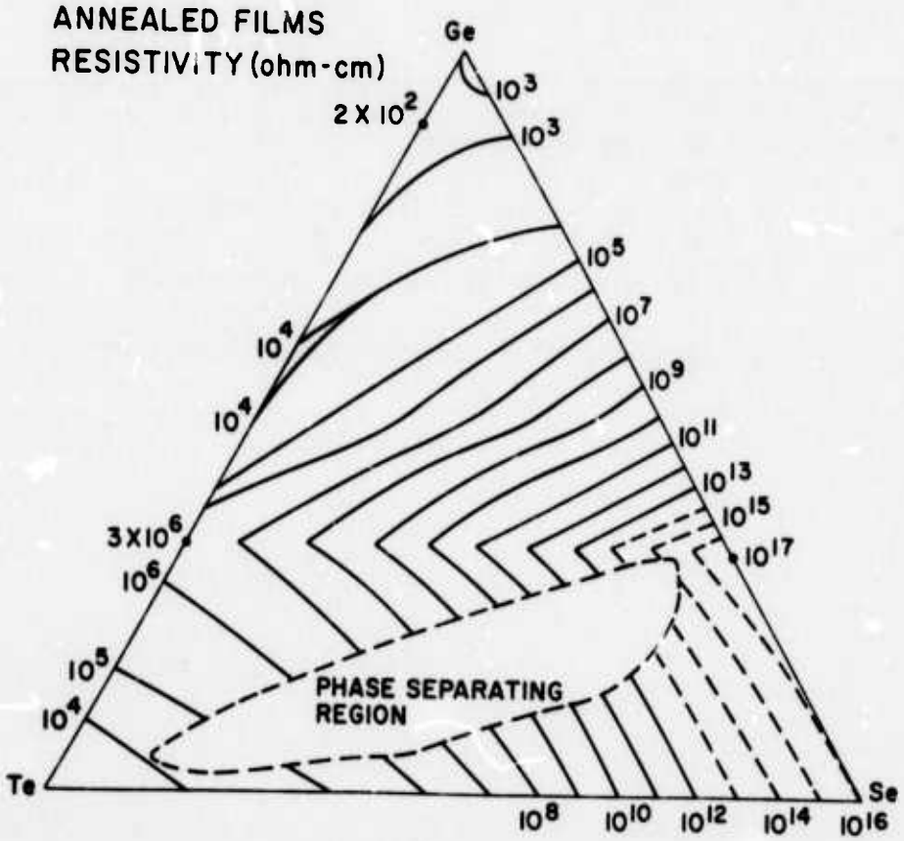
ANNEALED FILMS
RESISTIVITY (ohm-cm)
Ge
Te
Se
2×10^2
10^3
10^3
10^4
10^4
10^5
10^7
10^9
10^{11}
10^{13}
10^{15}
10^{17}
3×10^6
10^6
10^5
10^4
PHASE SEPARATING
REGION
10^8
10^{10}
10^{12}
10^{14}
10^{16}

these high resistivities at room temperature are estimated from high temperature extrapolations. Homogeneous annealed alloys are unobtainable in the phase separating region.

4.4 Summary and Conclusions

Extrema in electrical and optical properties were found along the entire $GeTe_2$-$GeSe_2$ line of the Ge-Te-Se ternary, for annealed films. These extrema are associated with the strength (and partial ionic character) of the germanium-chalcogen bond and the fact that along this pseudobinary line all bonds can be between Ge and chalcogen atoms, with Ge in four-fold and the chalcogen in two-fold coordination. The structure is presumed similar to that of vitreous silica, as exemplified by the Evans-King random network model.[49]

N-type thermopowers were discovered for annealed alloys from a large region of the ternary, suggesting the possibility of fabricating amorphous chalcogenide semiconductor devices employing n-type as well as p-type layers. By control of annealing steps, either n- or p-type conduction can be obtained in the same composition for a sizeable range of compositions.

Two factors were discovered which give a general trend from p- to n-type conduction: 1) annealing of the sputtered films increases the tendency toward n-type behavior, particularly for alloys containing selenium; and 2) increasing the Se:Te ratio increases the tendency toward n-type behavior in the annealed alloys.

BIBLIOGRAPHY

1. N. F. Mott, Advan. Phys. 16, 49 (1967)
2. A. Bienenstock, F. Betts and S. R. Ovshinsky, J. Non-Crystalline Solids 2, 347 (1970.
3. J. P. de Neufville, J. Non-Crystalline Solids 8-10, 85 (1972).
4. F. Betts, A. Bienenstock and S. R. Ovshinsky, J. Non-Crystalline Solids 4, 554 (1970).
5. F. Betts, A. Bienenstock, D. T. Keating and J. P. de Neufville, J. Non-Crystalline Solids 7, 417 (1972).
6. L. Pauling, Nature of the Chemical Bond. Cornell University Press, Ithaca, N.Y. (1960).
7. Ralph W. G. Wyckoff, Crystal Structures, Volume 1 and Volume 2, Interscience Publishers, New York (1964).
8. A. F. Wells, Structural Inorganic Chemistry, Oxford University Press, Oxford, England (1962).
9. H. Keller and J. Stuke, Phys. Stat. Sol. 8, 831 (1965).
10. J. Schottmiller, M. Tabak, G. Lucovsky and A. Ward, J. Non-Crystalline Solids 4, 80 (1970).
11. J. P. deNeufville, D. Sarrach, R. Seguin and J. Tyler, Bull. Amer. Cer. Soc., March (abs.) (1972).
12. J. P. deNeufville and D. Sarrach, Bull. Amer. Phys. Soc. 18, 421 (abs.) (1973).
13. N. J. Shevchik and W. Paul, J. Non-Crystalline Solids. 8-10, 381 (1972).

14. S. C. Moss and J. F. Graczyk, Proc. Intern. Conf. Physics of Semiconductors, Cambridge, Mass, 658 (1970).

15. E. A. Fagen, Abstract submitted to Fifth International Conference on Amorphous and Liquid Semiconductors.

16. H. K. Rockstad and J. P. deNeufville, Abstract submitted to Fifth International Conference on Amorphous and Liquid Semiconductors.

17. A. Eisenberg, personal communication (1973).

18. A. Eisenberg, Polymer Letters 1, 177 (1963).

19. J. P. deNeufville, C. H. Drummond and D. Turnbull, Phys. and Chem. Glasses 11, 186 (1970).

20. N. K. Abrikosov, V. F. Bankina, L. V. Poretskaya, L. E. Shelimova, and E. V. Skudnova, Semiconducting II-IV, IV-VI and V-VI Compounds, Monographs is Semiconductor Physics, Plenum Press, New York (1969).

21. R. Messier and R. Roy, Mat. Res. Bull. 6, 749 (1971).

22. F. A. Shunk, Constitution of Binary Alloys, Second Supplement, 394, McGraw-Hill, New York (1969).

23. M. Hansen, Constitution of Binary Alloys, 1188-1189, McGraw-Hill, New York (1958).

24. J. E. Morral, Ph.D. thesis, Dept. of Metallurgy and Materials Science, Mass. Inst. Tech., Cambridge, Mass. 02139 (1968).

25. M. B. Myers and J. S. Berkes, J. Non-Crystalline Solids 8-10, 804 (1972).

26. J. J. Mecholsky, G. R. Srinivasan, C. T. Moynihan and P. B. Macedo, J. Non-Crystalline Solids 11, 331 (1973).

27. R. Roy and V. Caslavaska, Solid State Commun. 7, 1467 (1969).

28. C. T. Moynihan, P. B. Macedo, I. D. Aggarwal and U. E. Schnaus, J. Non-Crystalline Solids 6, 322 (1971).

30. R. A. Powell and W. E. Spicer, Bull. Amer. Phys. Soc. 18, 390 (1973).

31. Second Semiannual Technical Report, Contract DAHC 15-70-C-0187, Advanced Research Projects Agency, Washington, D.C. (1970).

32. S. V. Nemilov, Zh. Prikl. Khimii No. 37, 1020 (1964).

33. A. Felz, H. J. Buttner, F. J. Lippmann and W. Maul, J. Non-Crystalline Solids 8-10, 64 (1972).

34. Y. Kawamoto and S. Tsuchihashi, J. Amer. Ceram. Soc. 54, 131 (1971).

35. M. B. Myers and E. J. Felty, Mater. Res. Bull. 2, 535 (1967).

36. R. Mozzi and B. E. Warren, J. Appl. Cryst. 2, 164 (1969).

37. E. Lorch, J. Phys. (C) 2, 229 (1969).

38. E. F. Riebling, J. Amer. Ceram. Soc. 51, 406 (1968).

39. O. V. Mazurin and M. V. Streltsina, J. Non-Crystalline Solids 11, 199 (1972).

40. R. D. Maurer, Symposium on Nucleation and Crystallization in Glasses and Metals, P. 5, The American Ceramic Society, Columbus, Ohio (1962).

41. D. Turnbull, J. Appl. Phys. 21, 1022 (1950).

42. S. D. Stookey, U.S. Patent 2, 920, 971 (1960).

43. B. E. Warren, X-ray Diffraction, Addison-Wesley (1969).

44. A. L. Luo and P. Duwez, Appl. Phys. Letters 2, 21 (1963).

45. J. E. Enderby and E. W. Collings, J. Non-Crystalline Solids 4, 161 (1970).

46. W. B. Hillig in Symposium on Nucleation and Crystallization in Glasses and Melts (American Ceramic Society, Columbus, Ohio, 1962) p. 77.

47. H. K. Rockstad and J. P. deNeufville, Proceedings of the 11th International Conference on the Physics of Semiconductors, (Polish Scientific Publishers, Warsaw, 1972), p. 542.

48. H. K. Rockstad and R. Flasck, "Transport and Optical Properties of Amorphous $(GeTe_2)_{1-x}$ $(GeSe_2)_x$ Alloy Films", to be submitted for publication. See also Appendix II, Final Technical Report of ARPA Contract DAHC15-70-C-0187.

49. D. L. Evans and S. V. King, Nature 212, 1353 (1966).

50. G. Lucovsky (personal communication, 1973) has been able to characterize the I.R. Spectra of these two alloys in terms of the expected scaling of the oscillater strengths observed for restriallin vibrations in SiO_2.

51. D. E. Polk, J. Non-Crystalline Solids 5, 365 (1971).

52. Powder Diffraction File, Inorganic Volume No. PDIS-5, 10iRB (Joint committee on Powder Diffraction Standards, Philadelphia, Pa., 1967).

53. S. C. Moss and J. P. deNeufville, Mat. Res. Bull. 7, 423 (1972).